

A plasmid-chromosome crosstalk in multidrug resistant enterobacteria

Received: 8 August 2024

Accepted: 3 December 2024

Published online: 30 December 2024



Laura Toribio-Celestino^{1,7}, Alicia Calvo-Villamañán ^{1,7}, Cristina Herencias^{2,3}, Aida Alonso-del Valle ¹, Jorge Sastre-Dominguez¹, Susana Quesada¹, Didier Mazel⁴, Eduardo P. C. Rocha ⁵, Ariadna Fernández-Calvet ¹ ✉ & Alvaro San Millán ^{1,6} ✉

Conjugative plasmids promote the dissemination and evolution of anti-microbial resistance in bacterial pathogens. However, plasmid acquisition can produce physiological alterations in the bacterial host, leading to potential fitness costs that determine the clinical success of bacteria-plasmid associations. In this study, we use a transcriptomic approach to characterize the interactions between a globally disseminated carbapenem resistance plasmid, pOXA-48, and a diverse collection of multidrug resistant (MDR) enterobacteria. Although pOXA-48 produces mostly strain-specific transcriptional alterations, it also leads to the common overexpression of a small chromosomal operon present in *Klebsiella* spp. and *Citrobacter freundii* strains. This operon includes two genes coding for a pirin and an isochorismatase family proteins (*ppf* and *ifp*), and shows evidence of horizontal mobilization across Proteobacteria species. Combining genetic engineering, transcriptomics, and CRISPRi gene silencing, we show that a pOXA-48-encoded LysR regulator is responsible for the plasmid-chromosome crosstalk. Crucially, the operon overexpression produces a fitness benefit in a pOXA-48-carrying MDR *K. pneumoniae* strain, suggesting that this crosstalk promotes the dissemination of carbapenem resistance in clinical settings.

Antimicrobial resistance (AMR) is becoming a leading global health problem, with AMR infections increasing every year^{1,2}. Conjugative plasmids are extrachromosomal genetic elements that can carry diverse accessory genes, including AMR genes, and can transfer them horizontally to nearby cells³. Many conjugative plasmids have a broad host range and can thus rapidly disseminate AMR genes across bacterial species⁴. This is especially relevant in clinical settings, where antibiotic pressure persistently selects for AMR plasmid-carrying bacteria⁵. One of the most concerning groups of resistant bacteria

are carbapenemase-producing Enterobacteriaceae (CPE)⁶. CPE are able to hydrolyze carbapenems, an important group of antibiotics typically used in hospitals as a last-resort option to treat multidrug resistant (MDR) infections. There are many types of globally disseminated carbapenemases⁶. One relevant example is OXA-48, which is usually encoded within a TnI999 composite transposon in the conjugative plasmid pOXA-48 (plasmid taxonomic unit L/M⁷, IncL incompatibility group⁸). The TnI999 transposon putatively mobilized the *bla*_{OXA-48} gene from the chromosome of the marine bacterial genus *Shewanella*

¹Centro Nacional de Biotecnología (CNB-CSIC), Madrid, Spain. ²Servicio de Microbiología, Hospital Universitario Ramón y Cajal and Instituto Ramón y Cajal de Investigación Sanitaria, Madrid, Spain. ³Centro de Investigación Biológica en Red de Enfermedades Infecciosas, Instituto de Salud Carlos III, Madrid, Spain. ⁴Institut Pasteur, Université de Paris Cité, CNRS UMR3525, Bacterial Genome Plasticity, Paris, France. ⁵Institut Pasteur, Université de Paris Cité, CNRS UMR3525, Microbial Evolutionary Genomics, Paris, France. ⁶Centro de Investigación Biológica en Red de Epidemiología y Salud Pública, Instituto de Salud Carlos III, Madrid, Spain. ⁷These authors contributed equally: Laura Toribio-Celestino, Alicia Calvo-Villamañán. ✉ e-mail: ariadna.fernandez@cnb.csic.es; asanmillan@cnb.csic.es

spp. into pOXA-48, which was first identified in a *Klebsiella pneumoniae* isolate in Turkey in 2001^{9,10}, and is currently involved in hospital outbreaks worldwide^{6,11}. Importantly, although pOXA-48 can be carried by many enterobacterial species, it is strongly associated with certain high-risk clones of *K. pneumoniae* (e.g. of the sequence type ST11)^{12,13}. Understanding the bacteria-plasmid interactions that shape these successful associations is crucial to controlling AMR dissemination.

When plasmids are acquired by a new bacterial host, they usually disrupt the cell's transcriptional profile, and this can translate into a fitness cost^{14,15}. Chromosomal genes with altered expression are normally related to the metabolism of nucleotides, amino acids and energy sources, translation and transcription, secretion and transport systems, signaling and motility^{14,16–25}. These transcriptional changes could just reflect side effects of plasmid carriage or readjustments made to compensate for the new energy requirements and the disruption of cellular homeostasis that result from expressing foreign genes^{15,26}. For instance, fitness costs associated with carriage of the pQBR103 or pQBR57 megaplasmids of *Pseudomonas fluorescens* are relieved by mutations in the global regulatory system GacAS, which restore the plasmid-free transcriptional profile^{17,27}.

Moreover, there is growing evidence that plasmids may modulate transcriptome changes to manipulate the bacterial host behavior as a strategy to increase their own transmissibility^{14,28}. Plasmids have been repeatedly described to reduce the expression of chromosomal genes related to bacterial motility^{18,29,30}, presumably to facilitate physical interaction with potential recipients for conjugation¹⁴. Interestingly, plasmids can employ other strategies to reduce bacterial motility, including translational regulation³¹, or direct protein interactions with the flagella³². Other transcriptional modulations could aim at increasing the fitness of the host in new niches to ultimately ensure the plasmid's vertical transmission^{14,28}. For example, plasmid pLL35 induces an increase in the expression of genes involved in anaerobic metabolism in *Escherichia coli*, which could help the host bacterium to colonize the mammalian gut²². Moreover, different virulence plasmids have been reported to regulate the expression of chromosomal genes associated with increased virulence^{33–36} or parasitic intracellular growth³⁷, promoting a pathogenic lifestyle. All these bacteria-plasmid interactions ultimately shape plasmid distribution and evolution. However, despite the importance of plasmids in the evolution of AMR, we are only starting to understand the transcriptional impact of AMR plasmids on their bacterial hosts, and very few studies have analyzed the effects of relevant AMR plasmids on clinically relevant bacterial strains^{19,22,29,38–41}.

In this study, we analyzed the transcriptional response associated with carrying plasmid pOXA-48 in 11 MDR enterobacterial strains of four different species isolated from hospitalized patients. Our analyses revealed that pOXA-48 produces variable responses on their hosts, but commonly affects processes related to metabolism, transport, cellular organization and motility. More notably, we demonstrated that a pOXA-48-encoded LysR transcriptional regulator directly increases the expression of a small chromosomal operon in *Klebsiella* spp. and *Citrobacter freundii*. This operon showed signs of having been horizontally mobilized across Proteobacteria, suggesting that interactions between mobile genetic elements may shape the evolution of plasmid-mediated AMR in clinically relevant enterobacteria. Moreover, our results suggest that the plasmid-chromosome crosstalk produces a fitness benefit in pOXA-48-carrying MDR strains.

Results

Transcriptomic analysis of pOXA-48-carrying MDR enterobacteria

To study the transcriptional impact of pOXA-48 carriage in clinically relevant bacteria, we analyzed 11 MDR enterobacterial strains isolated from the gut microbiota of patients admitted to a large University Hospital in Madrid, Spain (Supplementary Data 1 and Supplementary

Fig. 1). These 11 strains belong to four different species (*K. pneumoniae*, $n = 7$; *E. coli*, $n = 2$; *K. variicola*, $n = 1$; *C. freundii*, $n = 1$, Supplementary Fig. 1A) and are representative of the phylogenetic diversity of MDR enterobacteria isolated in this hospital (see methods)¹³. We also included in our analyses the laboratory-adapted *E. coli* MG1655 strain. As observed in our previous studies on the distribution of fitness effects of pOXA-48 in wild-type enterobacteria, pOXA-48 produced a wide range of fitness effects in these strains (Supplementary Fig. 1B)^{42,43}. For each strain, we had previously obtained pOXA-48-free and pOXA-48-carrying isogenic clones by curing (using CRISPR-Cas9 technology; strains C325, CF13, J57, H53 and K147) or introducing (by conjugation; strains EC10, MG1655, KPN04, KPN07, KPN10, KPN15 and KPN18) this plasmid^{42–44}. To perform the differential expression (DE) analysis, we sequenced the transcriptomes of all clones (pOXA-48-carrying and pOXA-48-free, $n = 24$ clones, 2–4 biological replicates per clone, see Methods).

Conserved expression of pOXA-48 genes across strains

Although the structure and sequence of plasmid pOXA-48 is quite conserved across enterobacteria, we have previously described multiple pOXA-48 variants carrying different indels and/or SNPs⁴⁵. Therefore, we first performed variant calling on the transcriptomic data and confirmed that the polymorphisms identified in pOXA-48 did not alter expression of the affected genes (Fig. 1 and Supplementary Data 2 and 3). We identified SNPs upstream of the *repA* gene of pOXA-48 in all replicates of *K. pneumoniae* KPN07 and KPN10 and in one replicate of EC10 (Supplementary Data 2). These mutations, which increase pOXA-48 copy number (PCN), have been previously described in nosocomial strains⁴⁵, so we decided to maintain them in the subsequent analyses.

Next, we analyzed the expression of pOXA-48 genes in the different genetic backgrounds of the 12 enterobacterial strains. Gene expression was calculated as Transcripts Per Million (TPM). To facilitate comparison between strains, TPM values were normalized by the median chromosomal TPM values of the corresponding strain. All plasmid genes were transcribed (Fig. 1, Supplementary Fig. 2 and Supplementary Data 3), in contrast to other AMR plasmids, where up to 40% of genes were silent^{19,46,47}. We did not observe distinctive transcriptional profiles of pOXA-48 associated with the different host genetic backgrounds. However, strains KPN07 and KPN10 and the replicate 3 of EC10 showed overall higher pOXA-48 expression (Fig. 1, Supplementary Fig. 2 and Supplementary Data 3), in agreement with the increased PCN caused by the mutation upstream *repA*. The most expressed gene was the carbapenemase *bla*_{OXA-48} (Fig. 1, Supplementary Fig. 2 and Supplementary Data 3). Other works have also reported AMR genes to be amongst the most expressed plasmid genes^{18,19,30,46,48}. Other highly transcribed genes were *traQ* and *traR*, involved in pilin formation and plasmid transfer, an H-NS-like regulatory protein-coding gene, and the toxin and antitoxin *pemK* and *pemI* genes, associated with plasmid maintenance through post segregational killing (Fig. 1 and Supplementary Data 3). The analysis of expression of other resident plasmid's genes is described in Supplementary Information.

Strain-specific transcriptomic changes associated with pOXA-48 carriage

pOXA-48 produced variable, strain-specific transcriptomic changes on the chromosome of its enterobacterial hosts (Supplementary Fig. 3). The number of differentially expressed genes (DEGs) ranged from only six in *K. pneumoniae* H53 to more than a thousand DEGs in the strains that carried a pOXA-48 variant with increased PCN (EC10, KPN07 and KPN10, 23–37% of total chromosomal genes) (Supplementary Data 4), which could reflect larger physiological alterations produced by the carriage of many copies of the plasmid. In the remaining MDR strains, pOXA-48 induced the DE of 2–15% of chromosomal genes

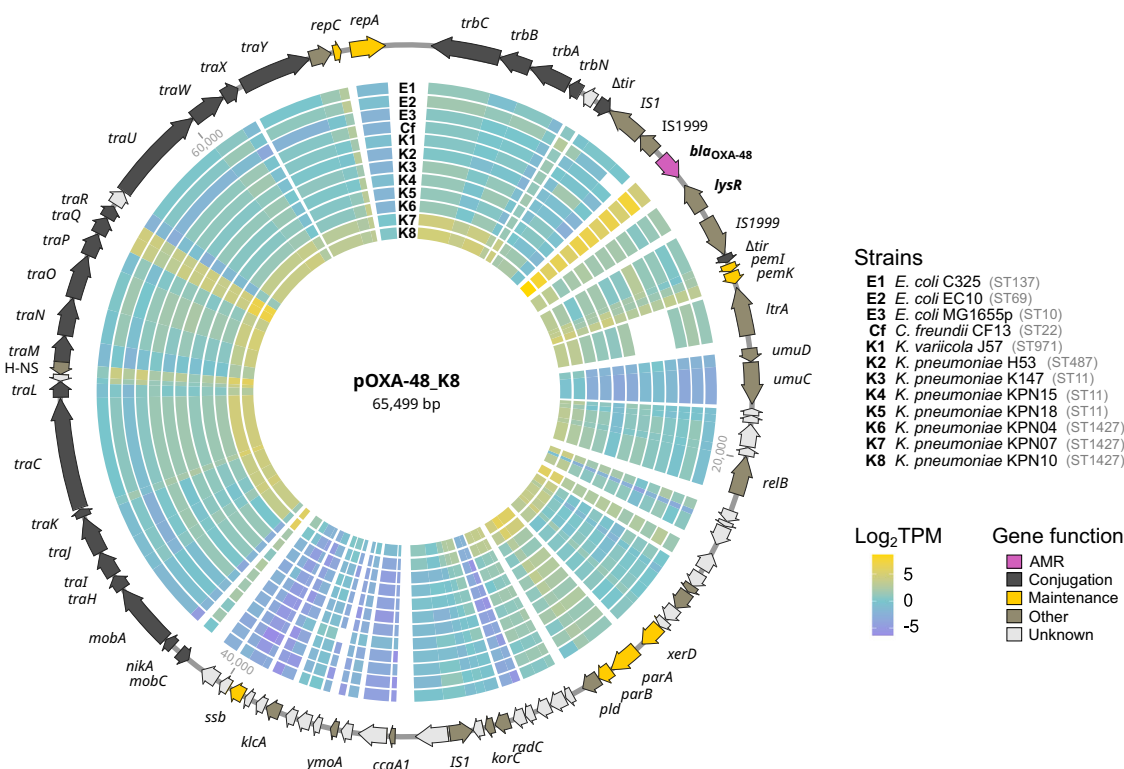


Fig. 1 | Expression of pOXA-48 genes. The genetic map of pOXA-48 shows the direction of transcription of genes as arrows, with colors indicating gene function. Each concentric circle of the heatmap represents the expression of pOXA-48 genes of each strain, measured as the median log₂TPM (Transcripts Per Million) between replicates, normalized by median chromosomal TPM values of the corresponding

strain. Log₂TPM > 0 indicates that pOXA-48 genes are expressed more than the median expression of chromosomal genes, while log₂TPM < 0 indicates that pOXA-48 gene expression is below the median chromosomal TPM values. Gaps in the heatmap mean that the pOXA-48 sequence of the reference genome does not include the gene or the gene was not annotated (see Supplementary Data 2).

(Supplementary Data 4). Several studies have also reported strain-specific transcriptional changes associated with plasmid carriage, which can be limited to only a small number of DEGs^{18,22,49}. Interestingly, only 63 genes were DE in the laboratory *E. coli* MG1655 strain (1.4% of total chromosomal genes) (Supplementary Data 4), which is surprising because pOXA-48 caused the highest fitness costs on this strain (Supplementary Fig. 1). However, in line with other studies^{22,24}, the number of DEGs did not correlate with the fitness cost imposed by pOXA-48 (Spearman's rank correlation, $\rho = -0.1$, $P = 0.75$, Supplementary Fig. 4).

To find commonly enriched functions between strains, we performed gene set enrichment analysis (GSEA) on the lists of raw DEGs with Gene Ontology (GO) functional annotations (Fig. 2, Supplementary Figs. 5 and 6 and Supplementary Data 5). We also counted the number of significant up- and downregulated genes for each GO Biological Process across strains (Supplementary Data 6). pOXA-48 carriage produced the most significant impact on host metabolism (Fig. 2, Supplementary Fig. 5 and Supplementary Data 5 and 6). The affected metabolic pathways and the extent of the changes varied across strains, but carbohydrate metabolism (including glycolysis and the TCA and glyoxylate cycles) and respiration (both aerobic and anaerobic, as well as the electron transport chain) were altered in multiple strains (Fig. 2 and Supplementary Data 5 and 6). This suggests that pOXA-48 could potentiate the exploration of alternative energy sources in its hosts, as seen for other plasmids^{22,24,25}. For example, nitrate assimilation and metabolism were upregulated in pOXA-48-carrying KPN07, EC10 and KPN10 (Fig. 2, Supplementary Fig. 5 and Supplementary Data 4, 5 and 6).

pOXA-48 also produced an overall impact in bacterial motility. Genes involved in flagella-dependent motility were strongly downregulated in 2 of the 3 *E. coli* strains: EC10 and MG1655 (Fig. 2,

Supplementary Fig. 6 and Supplementary Data 4, 5 and 6). Cell adhesion mediated by fimbriae tended to be downregulated in several strains, especially in *E. coli* EC10, *C. freundii* CF13 and *K. pneumoniae* KPN04 (Fig. 2, Supplementary Fig. 6 Supplementary Data 4, 5 and 6). Chemotaxis was also downregulated in EC10 and MG1655 (Fig. 2 and Supplementary Data 4, 5 and 6). Reduced motility is a common plasmid effect, which could facilitate its horizontal transmission through conjugation^{14,18,29,30}.

pOXA-48 induces the overexpression of a small and mobile chromosomal operon

Very few common genes were significantly DE across the strains, and those who were showed different directions of DE (Supplementary Fig. 3C and Supplementary Data 4). However, we observed a tuned overexpression of two adjacent chromosomal genes (*pfp* and *ifp*) coding for a pirin and isochorismatase family proteins in all *Klebsiella* spp. strains and in *C. freundii* (Fig. 3A, Supplementary Fig. 7 and Supplementary Data 4). Both genes were predicted to form a small operon (with a 97% probability as reported by Operon-mapper). A LysR family transcriptional regulator was encoded upstream of the operon, in antisense, and could therefore regulate its expression (Fig. 3A). From here on, we will refer to these three genes as the *lysR-pfp-ifp* cluster. Crucially, none of the *E. coli* strains encoded the *lysR-pfp-ifp* cluster (Fig. 3A).

A search on the STRING database revealed that the *lysR-pfp-ifp* cluster is present in many, but not all, species of Proteobacteria (Supplementary Fig. 8). This particular distribution led us to investigate the possible origin of the *lysR-pfp-ifp* cluster. For this, we used the RefSeq database of all non-redundant complete genomes of Proteobacteria ($n = 22,631$) and identified the *lysR-pfp-ifp* cluster in 5,983 Gamma- (18.6% of species), 191 Beta- (18.9% of species) and 172

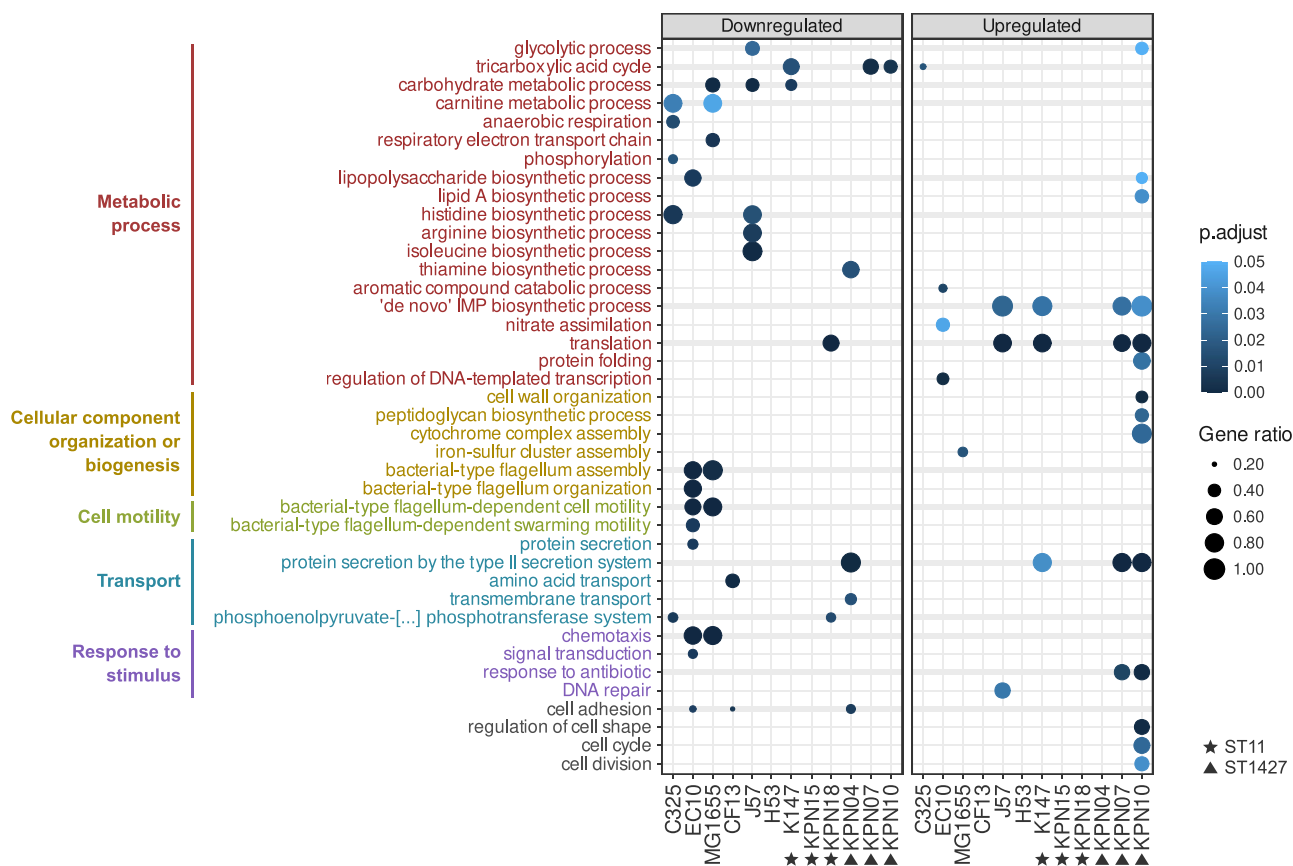


Fig. 2 | Transcriptomic responses to pOXA-48 carriage. Biological Processes (BP) enriched in pOXA-48-carrying enterobacteria. Gene set enrichment analysis (GSEA), correcting for multiple tests with the Benjamini-Hochberg procedure, was performed on the lists of raw DEGs annotated with Gene Ontology terms for BP (see Methods). Downregulated and upregulated enriched BP are separated in two panels, and are represented by circles. Thicker horizontal lines indicate BP enriched

in more than one strain. The size of the circles indicate the ratio of the number of enriched genes of a specific BP by the number of total genes annotated for that BP. The adjusted *p*-value for each enriched BP and strain is represented in a color gradient. Strains belonging to the same Sequence Type (ST) are indicated with shapes.

Alphaproteobacteria (8.8% of species) genomes (Supplementary Data 7; see Methods). Importantly, most strains of enterobacterial species typically associated with pOXA-48 (including >84% *Klebsiella* spp., >78% *Citrobacter* spp., >70% *Enterobacter* spp., >99% *Salmonella* spp. and >50% *Serratia* spp.) encoded a *lysR-pfp-ifp* cluster, except for *E. coli*, in which only two strains encoded the cluster (Supplementary Data 7). Genomes encoding only *pfp-ifp* clusters without the associated *lysR* gene were uncommon (see Methods). Next, we constructed a phylogenetic tree of 698 representative *lysR-pfp-ifp* cluster-encoding strains of Proteobacteria from the concatenated alignments of the LysR, PFP and IFP protein sequences (Fig. 3B). We also constructed a separate tree for each of the proteins (Supplementary Figs. 8, 9 and 10), which showed similar tree topologies, suggesting the three genes are evolutionarily related. Curiously, the tree of the *lysR-pfp-ifp* cluster did not branch according to the taxonomic class of the strains, but rather all clades included a mix of classes of Proteobacteria (Fig. 3B), suggesting the *lysR-pfp-ifp* cluster experienced frequent horizontal transfer. This was supported by ancestral character reconstruction, where the *lysR-pfp-ifp* cluster appeared at the tips of the tree and outer internal nodes in all classes of Proteobacteria, and was often absent in more internal nodes, suggesting horizontal acquisition (Supplementary Fig. 12).

In line with this hypothesis, the genes neighboring the *lysR-pfp-ifp* cluster differed between species of Proteobacteria, suggesting it could have been horizontally acquired and integrated at different genomic regions (Fig. 3C and Supplementary Fig. 13). Accordingly, of the 3,105 *E. coli* strains in the database, only two encoded a *lysR-pfp-ifp* cluster,

which was located near genes annotated as transposases of the IS3 family (Fig. 3B, C). The *lysR-pfp-ifp* cluster was also inserted between homologous tRNAs in different species (Fig. 3C), which are known integration sites for mobile genetic elements⁵⁰. Moreover, the *lysR-pfp-ifp* cluster showed different GC content (difference ranging from 0.4% to 9.2%, median 2.8%; Supplementary Data 8) and lower codon adaptation index compared to the host bacteria chromosomes for different species (median CAI between of *lysR* = 0.42, *pfp* = 0.57 and *ifp* = 0.6, median CAI of ribosomal genes = 0.76; Supplementary Data 8), further supporting the hypothesis of high horizontal mobility of the *lysR-pfp-ifp* cluster.

A pOXA-48-encoded LysR regulator increases the expression of the *pfp-ifp* operon

pOXA-48 encodes a LysR transcriptional regulator downstream the *bla*_{OXA-48} gene (Fig. 4A). Extensive evidence suggests that both *bla*_{OXA-48} and *lysR*_{pOXA-48} originate from the chromosome of *Shewanella* spp., and were trapped and mobilized into an IncL plasmid backbone by a Tn1999 composite transposon^{9,10} (see Supplementary Information for a detailed analysis of LysR_{pOXA-48} sequence conservation across pOXA-48 plasmids and a review of the Tn1999 variants). Notably, LysR_{pOXA-48} shows the highest protein sequence identity (34.2% in *C. freundii* and 36.7–37% in *Klebsiella* spp.) with the LysR that putatively regulates the expression of the *pfp-ifp* operon in comparison to other chromosomal LysRs (Supplementary Data 9). Thus, we hypothesized that LysR_{pOXA-48} could be activating the expression of the operon genes (Fig. 4A).

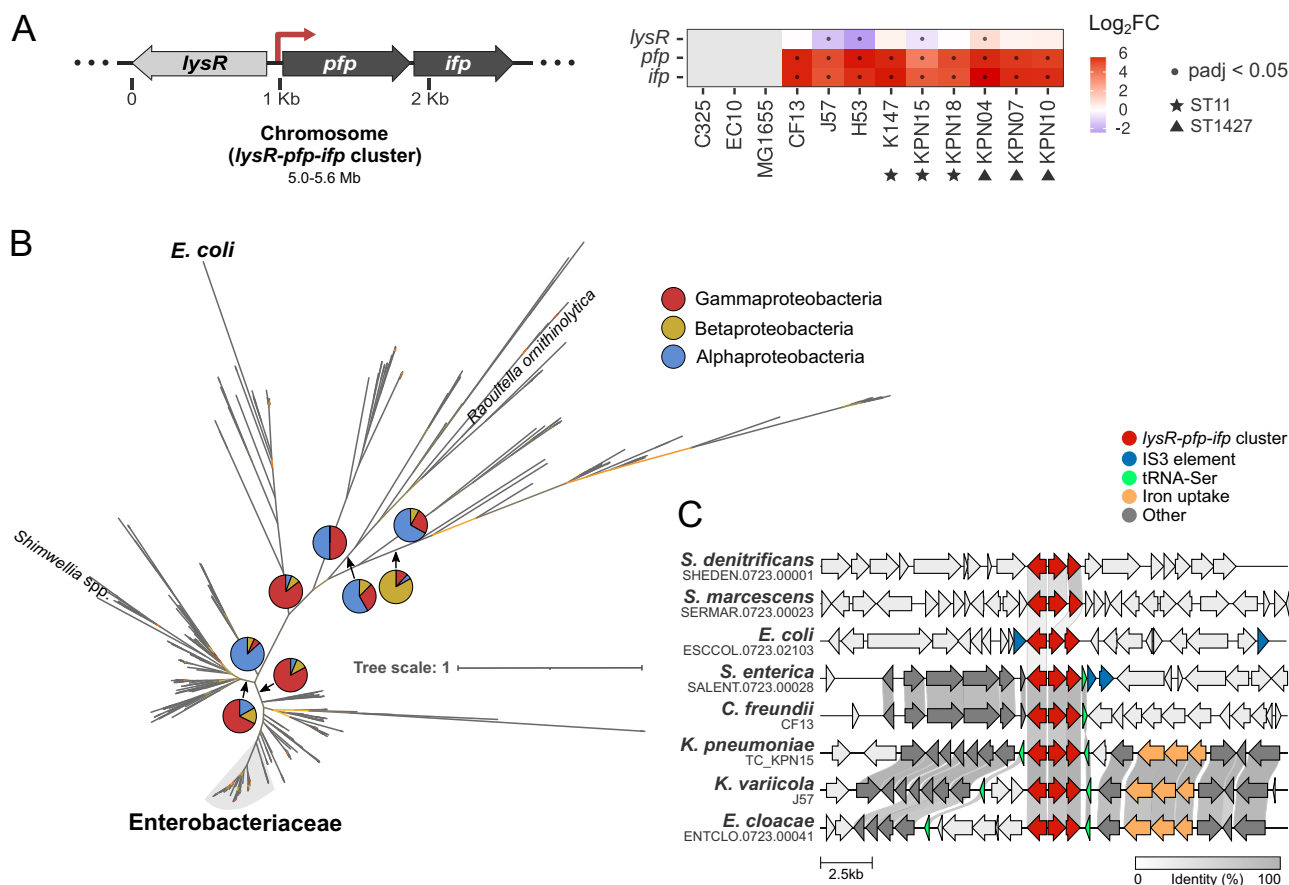


Fig. 3 | Overexpression of a small, horizontally-acquired, chromosomal operon. **A** Schematic representation (left panel) and heatmap of the differential expression (\log_2 fold change [FC], right panel) of a small chromosomal operon, comprised of the *pfp* and *ifp* genes, and the *lysR* transcriptional regulator gene that could control its expression (*lysR-pfp-ifp* cluster). Differential expression is performed by comparing the pOXA-48-carrying strains to their respective pOXA-48-free counterparts (see Methods). *E. coli* (C325, EC10 and MG1655) does not encode the *lysR-pfp-ifp* cluster, thus heatmap tiles are colored in gray. Significant \log_2 FC are indicated by a dot. Strains belonging to the same Sequence Type (ST) are indicated with shapes. **B** Unrooted phylogenetic tree of the concatenated alignments of the protein sequences of the *lysR-pfp-ifp* cluster genes in Proteobacteria ($n = 698$) (see Methods). Pie charts show the proportion of Proteobacteria strains belonging to

the Gamma- (red), Beta- (yellow) or Alphaproteobacteria (blue) classes included below each of the indicated internal branches. Enterobacteriaceae strains that branch from the same node are shaded in gray; other Enterobacteriaceae species not branching from that node are indicated. Bootstrap values are represented with a color gradient in the branches of the tree: low (approx. 8), medium (approx. 46) and high (approx. 100) bootstrap values are colored in red, yellow and gray, respectively. Tree scale represents the average number of substitutions per site. **C** Genomic neighborhood of the *lysR-pfp-ifp* cluster in a representative subset of Proteobacteria strains: *Shewanella denitrificans*, *Serratia marcescens*, *E. coli*, *Salmonella enterica*, *C. freundii*, *K. pneumoniae*, *K. variicola* and *Enterobacter cloacae*. Genes are color-coded as indicated at the top. Homologous genes between strains and their percentage of sequence identity are indicated with a gray shading.

To test this hypothesis, we constructed a version of pOXA-48 with *lysR*_{pOXA-48} interrupted by a kanamycin-resistance cassette (pOXA-48 Δ *lysR*, Fig. 4B) and conjugated it into two pOXA-48-free MDR strains: *K. pneumoniae* KPN15 and *C. freundii* CF13. No *E. coli* strain was included in this part of the study due to the absence of the *lysR-pfp-ifp* cluster in all of our *E. coli* strains. Using RT-qPCR, we compared the levels of expression of the *pfp-ifp* operon in the presence of pOXA-48 or pOXA-48 Δ *lysR*, and in the absence of either plasmid (Fig. 4D). Our results confirmed that the *pfp-ifp* operon is overexpressed (ca. 20-fold) in the presence of pOXA-48 (Dunnett's test $P = 0.0008$ for KPN15, $P = 0.034$ for CF13), but not in the presence of pOXA-48 Δ *lysR* (Dunnett's test $P = 0.3$ for KPN15 and $P = 0.3$ for CF13), compared to the plasmid-free strains, both for KPN15 and CF13 (Fig. 4D).

To complement the deletion of *lysR*, we constructed the expression vector pTet-*LysR* (Fig. 4C). This vector expresses *lysR*_{pOXA-48} under the control of the P_{tet} promoter, inducible by anhydrotetracycline (aTc). The *LysR*_{pOXA-48} expressed from the induced pTet-*LysR* vector led to the overexpression of the *pfp-ifp* operon, showing that *LysR*_{pOXA-48} is necessary and sufficient for the transcriptional activation of the

pfp-ifp operon (Fig. 4D). Additionally, our RT-qPCR results revealed that *LysR*_{pOXA-48} plays no role in the expression of *bla*_{OXA-48}, as levels of *bla*_{OXA-48} were similar using pOXA-48 or pOXA-48 Δ *lysR* (t -test, $t(1.19) = 0.49$, $P = 0.7$ for KPN15, $t(1.45) = -2.16$, $P = 0.21$ for CF13; Fig. 4D).

The *LysR*-mediated transcriptional regulation is specific to the operon genes

To further characterize the regulatory functions of *LysR*_{pOXA-48}, we sequenced the transcriptomes of *K. pneumoniae* KPN15 and *C. freundii* CF13, carrying pOXA-48 or pOXA-48 Δ *lysR*, and performed DE analysis. When analyzing the expression of pOXA-48 genes, none was DE in the same direction in both strains—including *bla*_{OXA-48}, in line with our RT-qPCR results—and the magnitude of DE was moderate (\log_2 FC ranging from -0.56 to 1.46 , Supplementary Data 10). This indicates that *LysR*_{pOXA-48} does not regulate the expression of any pOXA-48 gene.

The operon genes *pfp* and *ifp* were overexpressed when comparing the pOXA-48 carriers against the *LysR*_{pOXA-48}-deficient strains carrying pOXA-48 Δ *lysR*, further confirming that *LysR*_{pOXA-48} is

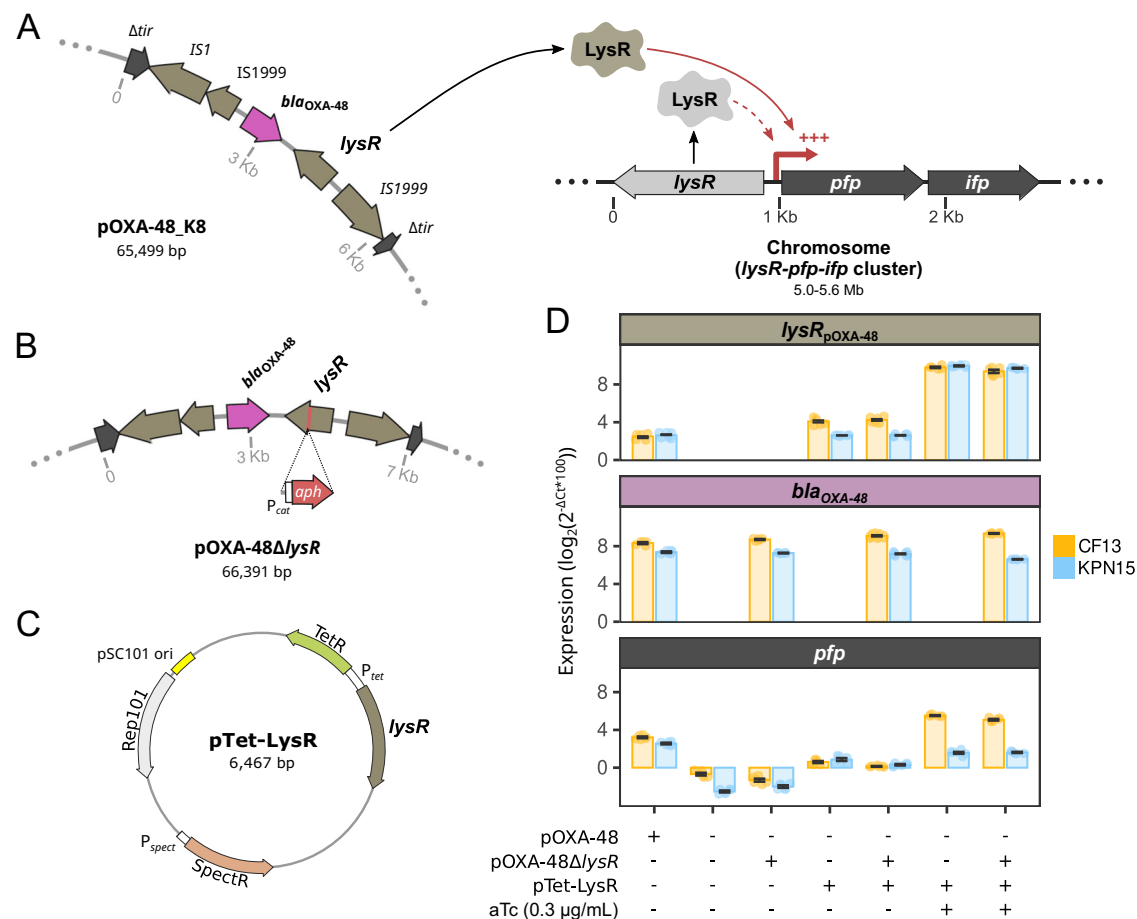


Fig. 4 | Plasmid-chromosome transcriptional crosstalk. **A** Schematic representation of the plasmid-chromosome crosstalk mediated by the pOXA-48-encoded LysR transcriptional regulator. In the presence of pOXA-48, the overexpression of the operon genes is mediated by LysR_{pOXA-48} (solid red arrow). The thick red arrow represents the putative promoter of the operon. Chromosome and plasmid are represented at different scales, indicated in the figure. **B** Zoom in on the pOXA-48ΔlysR plasmid. The *lysR* gene of pOXA-48 was knocked-out by inserting the *aph(3)-Ila* resistance gene. **C** Map of the pTet-LysR plasmid. The

expression of *lysR*_{pOXA-48} is controlled by the inducible promoter *P*_{tet}. **D** RT-qPCR results for the expression of *lysR*_{pOXA-48}, *bla*_{OXA-48} and the *pfp*-*ifp* operon (*pfp* levels as proxy for the entire operon). Levels of expression are normalized to the endogenous control *rpoB* and represented as the log₂FC of gene expression compared to *rpoB*. Error bars represent the standard error of the mean (*n* = 2 biological replicates, each as the median of 3 technical replicates). Source data are provided as a Source Data file.

responsible for the increased expression of the operon (mean log₂FC of *pfp* = 5.54 and *ifp* = 4.95; Fig. 5 and Supplementary Data 10). Apart from the operon genes, few other chromosomal genes were strongly DE (log₂FC ranging from -2.53 to 2.67, mean = 0.007) or were DE in the same direction in KPN15 and CF13 (Supplementary Data 10), suggesting that LysR_{pOXA-48} only activates the expression of the operon. To investigate this further, we analyzed the DE of genes that could be under the control of other LysR regulators. We considered a gene to be putatively controlled by a LysR if a *lysR* gene was located upstream and in antisense of the gene, as in the *lysR*-*pfp*-*ifp* cluster (Fig. 5). Only five genes putatively controlled by a LysR (excluding *pfp*) were significantly DE in CF13 and KPN15 (Fig. 5). However, they were only marginally DE (log₂FC ranging from -1.4 to 0.37) and none of them were DE in the same direction across strains when comparing pOXA-48 carriers against plasmid-free strains (Supplementary Data 4). These results suggest that the LysR-mediated plasmid-chromosome crosstalk is specific to the operon genes.

Functional analysis of the operon genes

Next, we decided to study the function of the *pfp*-*ifp* operon genes. Many members of the pirin family protein possess quercetinase activity, oxidizing the flavonoid quercetin⁵¹. To test the quercetinase activity of the PFP protein, we cultured *C. freundii* CF13 and *K.*

pneumoniae KPN15 carrying either pOXA-48 or pOXA-48ΔlysR in different concentrations of quercetin solubilized in DMSO (Fig. 6A and Supplementary Fig. 14). Quercetin possesses antimicrobial activity⁵², thus we hypothesized that if PFP degrades quercetin, strains carrying pOXA-48ΔlysR—producing less PFP—would present a growth defect compared to pOXA-48-carrying strains. By constructing a generalized additive model per strain (GAM; see Methods), we showed that, in KPN15, pOXA-48ΔlysR-carrying strains are more susceptible to quercetin than pOXA-48-carrying strains (Fig. 6A, Supplementary Fig. 15 and Supplementary Data 11), which strongly suggests that PFP has quercetinase activity in *K. pneumoniae*. In CF13, on the other hand, we did not observe a clear difference between pOXA-48- and pOXA-48ΔlysR-carrying strains (Fig. 6A, Supplementary Fig. 15 and Supplementary Data 11).

Members of the isochorismatase-like superfamily, like the EntB enzyme involved in enterobactin biosynthesis, typically hydrolyze the isochorismate to 2,3-dihydroxybenzoate and pyruvate. Enterobactin is a high-affinity bacterial siderophore involved in iron uptake⁵³. Interestingly, when comparing pOXA-48-carrying to -free strains, we observed a tendency to overexpress genes related to iron uptake in the *E. coli* strains—that lack the operon—and *K. pneumoniae* KPN07 and KPN10 MDR strains—with higher PCN—(Fig. 6B and Supplementary Fig. 16), suggesting an increased pOXA-48-dependent iron demand in

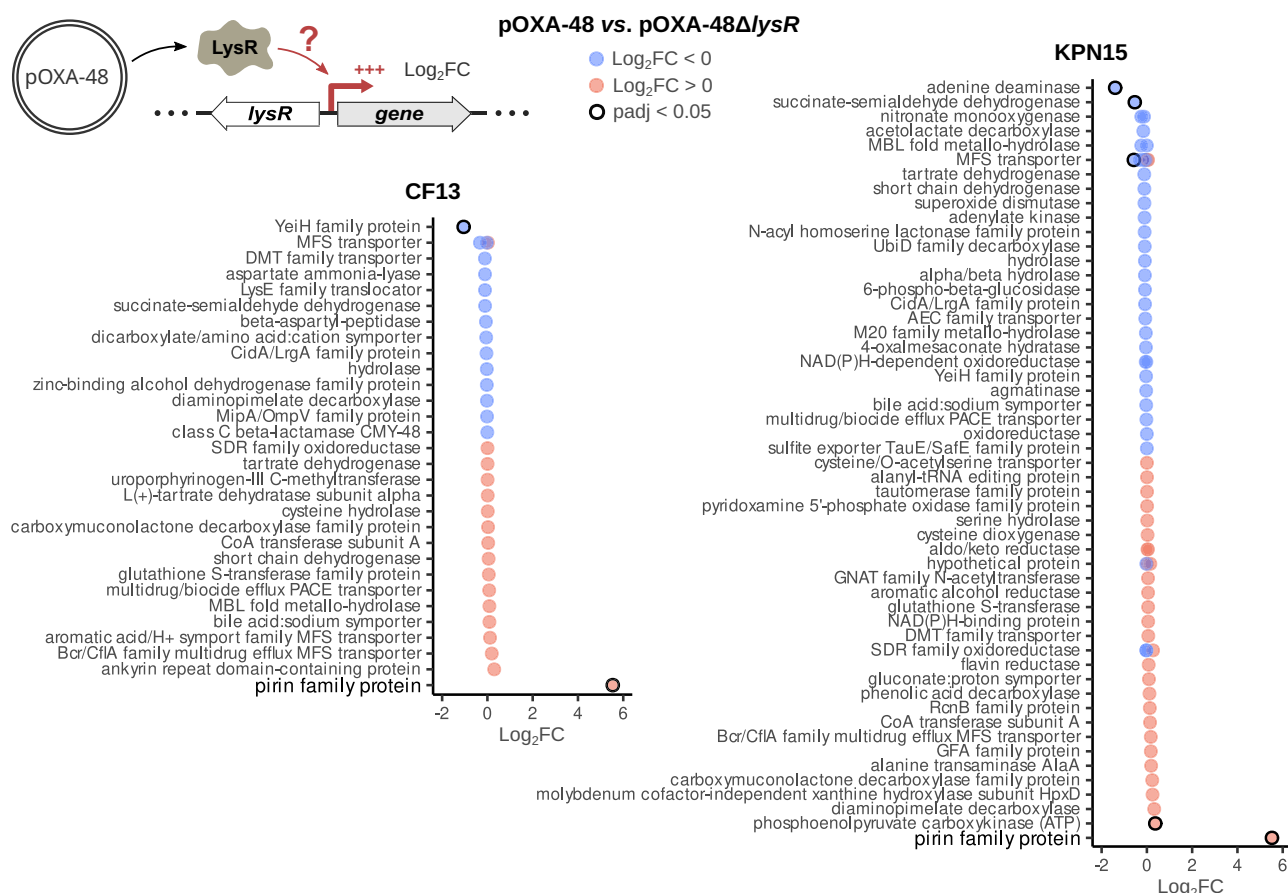


Fig. 5 | Differential expression of chromosomal genes putatively controlled by other LysRs. Genes were considered to be potentially regulated by a LysR transcriptional regulator if a *lysR* gene was preceding the gene in antisense (top schematic representation). The log₂FoldChanges (comparing pOXA-48-carrying to pOXA-48ΔlysR-carrying counterparts) of the genes (represented as gene products)

putatively controlled by LysRs are plotted for CF13 (left) and KPN15 (right). The pirin family protein of the *lysR-pfp-ifp* cluster is emphasized. Red and blue circles represent up- and downregulation, respectively. Outlined circles indicate significant log₂FC (adjusted *p*-value < 0.05).

these strains. This tendency was also observed in KPN15 and CF13 carrying the pOXA-48ΔlysR variant compared to the strains carrying pOXA-48 (Fig. 6C). Moreover, in this last comparison, KPN15/pOXA-48ΔlysR also downregulated the expression of *fur*, a global ferric uptake transcriptional repressor (Fig. 6C). Thus, we hypothesized that IFP could be related to the enterobactin biosynthetic pathway, increasing enterobactin-mediated iron uptake and compensating an increased iron demand caused by pOXA-48 carriage. To determine whether overexpression of the *pfp-ifp* operon increases iron uptake, we measured growth of CF13 and KPN15 under increasing concentrations of the iron chelator bipyridine (Supplementary Fig. 17). However, we did not observe any growth difference in strains carrying pOXA-48 or pOXA-48ΔlysR in iron-deficient conditions (Supplementary Fig. 17). The regulation of iron transport is complex, with many different systems involved in iron acquisition. It is therefore possible that the observed adjustments in expression of genes involved in iron import (Fig. 6B, C) could be compensating for the underexpression of the *pfp-ifp* operon, increasing iron acquisition in the pOXA-48ΔlysR-carrying strains.

Overexpression of the *pfp-ifp* operon increases the fitness of a pOXA-48-carrying strain

To investigate the biological relevance of the *pfp-ifp* operon, we first measured the fitness effects associated with *pfp-ifp* overexpression in pOXA-48-free strains. We performed growth curves for both *C. freundii* CF13 and *K. pneumoniae* KPN15 carrying the pTet-LysR vector, which

induction leads to *pfp-ifp* expression (Fig. 7A, Supplementary Fig. 18). As a proxy for fitness, we measured the area under the growth curve (AUC) at different levels of aTc induction (note that even with no aTc there is a leaky expression from pTet-LysR, see Fig. 4D). In CF13, aTc produced a moderate growth arrest (one-way ANOVA, CF13: $F(3,16) = 22.45$, $P < 0.001$; KPN15: $F(3,16) = 0.042$, $P = 0.99$), which complicated the interpretation of the results in this strain. Overall, we observed that pTet-LysR produced a beneficial effect in CF13 and a detrimental effect in KPN15, across different aTc concentrations (two-way ANOVA for the interaction between aTc concentration and pTet-LysR, CF13: $F(3,32) = 7.60$, $P < 0.001$; KPN15: $F(3,32) = 4.31$, $P = 0.014$; for Tukey's multiple comparisons tests see Supplementary Data 11).

To directly study the effect of *pfp-ifp* overexpression in the pOXA-48-carrying strains, we constructed a CRISPRi system able to silence the *pfp-ifp* operon. The pFR56apm vector carries *Streptococcus pyogenes*' dCas9 under the control of a pHlf promoter, and is easily reprogrammable to target any desired DNA locus by changing an sgRNA which is constitutively expressed. To silence the *pfp-ifp* operon, we designed an optimal sgRNA against the first gene of the operon, *pfp*, using a guide activity predictor⁵⁴. By silencing the first gene in an operon the entire operon is silenced as a polar effect of the CRISPRi mechanism⁵⁵. We performed experiments in both *C. freundii* CF13 and *K. pneumoniae* KPN15. However, RT-qPCR results for *pfp* expression showed that our CRISPRi set-up did not lead to a strong gene silencing in CF13 (Supplementary Fig. 19), so we focused our work on the KPN15 background, where CRISPRi mediated silencing was efficient (Fig. 7B).

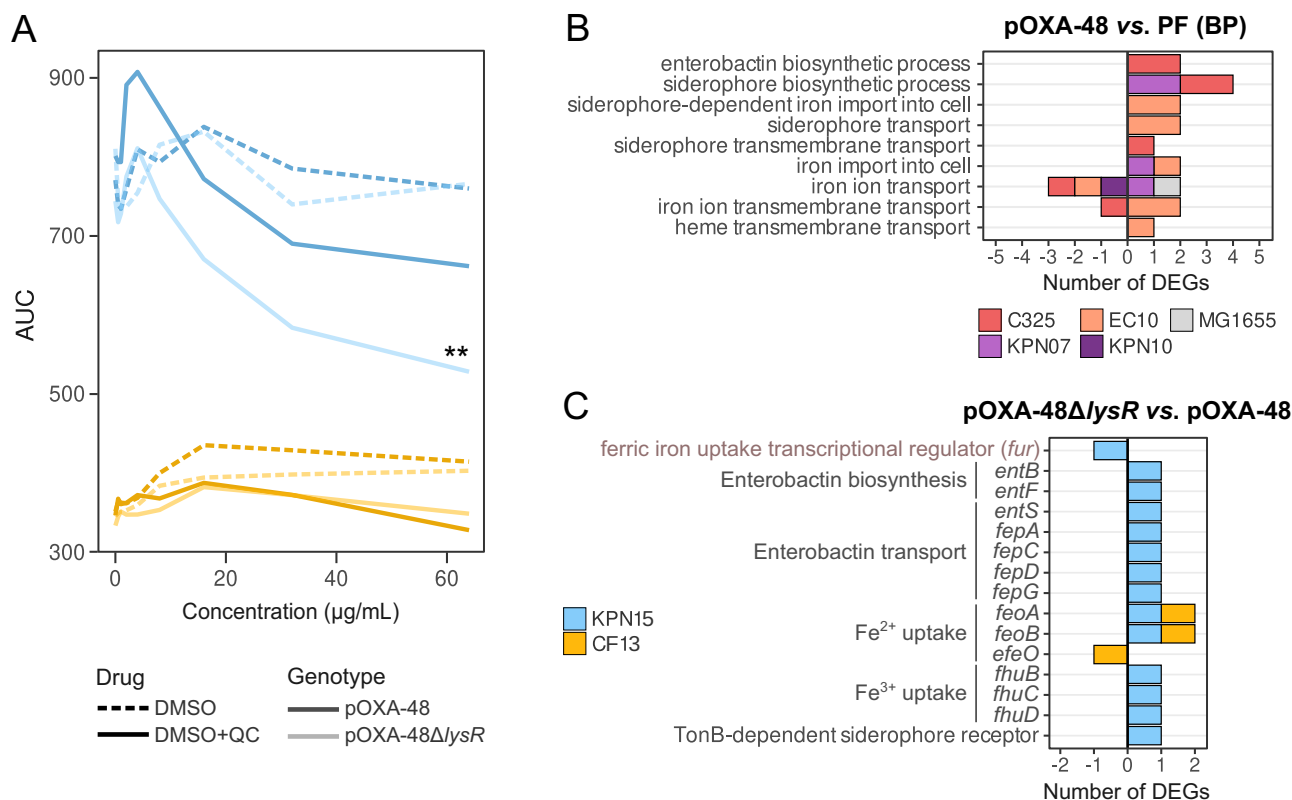


Fig. 6 | Functional analysis of the operon genes. A AUC of growth curves under increasing concentrations of DMSO or DMSO + quercetin (QC) of KPN15 and CF13 carrying pOXA-48 or pOXA-48 ΔlysR ($n = 1$ for DMSO and $n = 2$ for DMSO + QC). This data was used to construct a GAM per strain (Supplementary Fig. 15; see Methods). Asterisks represent statistical significance: * $P \leq 0.05$, ** $P \leq 0.01$, *** $P \leq 0.001$. **B** Number of significant DEGs annotated with biological processes (BP) related to iron transport (comparing pOXA-48-carrying against pOXA-48-free [PF] strains of

the first RNA-Seq dataset). Note that genes annotated with more than one of the represented BP will be counted once in each BP. **C** Number of significant DEGs involved in iron transport (comparing pOXA-48 ΔlysR -carrying against pOXA-48-carrying strains of the second RNA-Seq dataset). In B and C, values > 0 represent the count of upregulated genes, and values < 0 are downregulated genes. Source data are provided as a Source Data file.

Our results showed that silencing the *pfp-ifp* operon has no significant fitness effect on the plasmid-free (Tukey's post-hoc test, coefficient = 4.46, $P = 0.99$) and pOXA-48 ΔlysR -carrying KPN15 (Tukey's post-hoc test, coefficient = -30.08, $P = 0.25$; Fig. 7C, Supplementary Fig. 19 and Supplementary Data 11), probably due to the operon's low level of constitutive expression (Figs. 4D and 7B). In the pOXA-48-carrying strain, on the other hand, silencing the *pfp-ifp* operon produced a clear decrease in fitness (Tukey's post-hoc test, coefficient = -166., $P < 0.001$; Fig. 7C, Supplementary Fig. 19 and Supplementary Data 11). These results suggest that *pfp-ifp* overexpression increases the fitness of the pOXA-48-carrying strain, which actually shows a higher AUC than the plasmid-free (Tukey's post-hoc test, coefficient = 84.43, $P < 0.001$; Fig. 7C, Supplementary Fig. 19 and Supplementary Data 11) and pOXA-48 ΔlysR -carrying strains (Tukey's post-hoc test, coefficient = -106.61, $P < 0.001$; Fig. 7C, Supplementary Fig. 19 and Supplementary Data 11) in these experimental conditions.

In light of these results, we hypothesized that the overexpression of the *pfp-ifp* operon could be also beneficial for the pOXA-48 ΔlysR -carrying KPN15 and CF13 strains. To test this hypothesis, we performed growth curves of KPN15 and CF13 carrying both pOXA-48 ΔlysR and pTet-LysR under different levels of aTc induction (Fig. 7A, Supplementary Fig. 18). Our results showed a clear beneficial effect associated with pTet-LysR carriage in CF13, especially at high induction levels (two-way ANOVA for the interaction between aTc concentration and pTet-LysR, $F(3,32) = 7.98$, $P < 0.001$; for Tukey's multiple comparisons tests see Supplementary Data 11). For KPN15, we observed an overall growth deficit associated with pTet-LysR (two-way ANOVA for the

interaction between aTc concentration and pTet-LysR; $F(3,32) = 5.43$, $P = 0.004$; for Tukey's multiple comparisons tests see Supplementary Data 11). However, this defect disappeared at the lowest aTc concentration tested ($0.075 \mu\text{g/mL}$, Tukey's post-hoc test, coefficient = 45.27, $P = 0.69$), suggesting that this particular level of expression may be beneficial for pOXA-48 ΔlysR -carrying KPN15.

If overexpression of the *pfp-ifp* operon actually increased the fitness of pOXA-48-carrying enterobacteria, we would expect to find the plasmid more frequently associated with operon-encoding strains. Thus, we tested this possible association in the RefSeq genomes of enterobacterial genera where pOXA-48 is usually isolated (*Klebsiella* spp., *Escherichia* spp., *Enterobacter* spp., *Citrobacter* spp., *Salmonella* spp. and *Serratia* spp., $n = 8,125$ genomes, $n = 173$ carrying pOXA-48, $n = 4,752$ encoding the *pfp-ifp* operon; see Methods). We found that 3.1% of strains encoding the *pfp-ifp* operon carried pOXA-48, while only 0.8% strains lacking the operon carried the plasmid. Importantly, the association between encoding the *pfp-ifp* operon and carrying pOXA-48 was significant (χ^2 test with Yates' continuity correction, $\chi^2 = 46.23$, $P = 1.06 \times 10^{-11}$), supporting that overexpression of the *pfp-ifp* operon is beneficial for pOXA-48-carrying enterobacteria.

Discussion

The complex interactions that occur between plasmids and their hosts shape the evolution of AMR. These interactions can disrupt cellular processes at multiple levels, including the host's transcriptional regulation. In this work, we explored the impact of the carbapenem-resistance plasmid pOXA-48 on the transcriptomes of 11 MDR

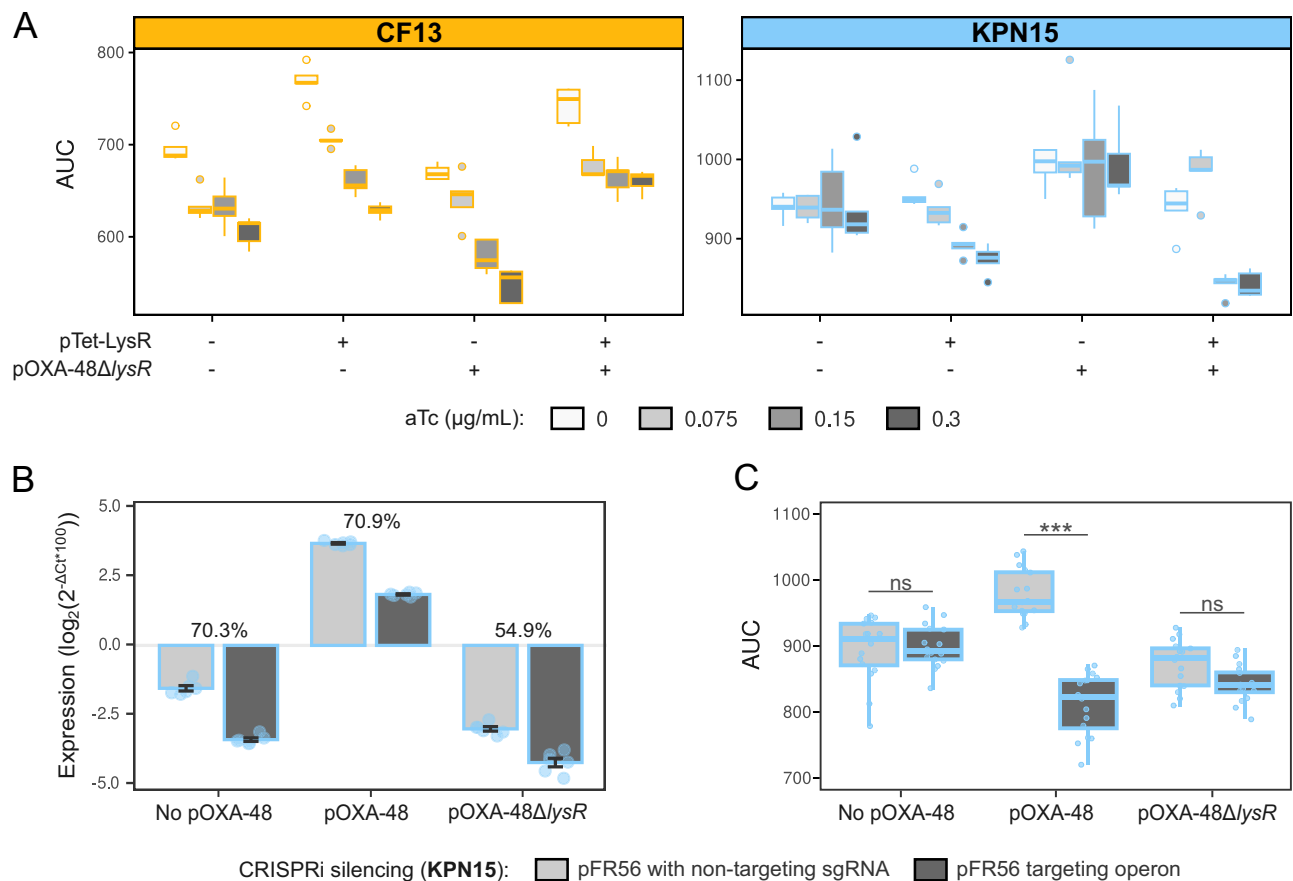


Fig. 7 | Analysis of the overexpression and repression of the *pfp-ifp* operon.

A Effect of the overexpression of *LysR_{pOXA-48}* on the growth of CF13 and KPN15. AUC of plasmid-free and pOXA-48ΔlysR-carrying CF13 and KPN15, with expression of *LysR_{pOXA-48}* in *trans* from the pTet-LysR ($n = 5$ replicates for each strain/condition pairing). Experiment performed with increasing concentrations of inducer (aTc). **B** Effect of CRISPRi repression on the expression of the *pfp-ifp* operon. RT-qPCR results for *pfp* as proxy of the whole operon, normalized to the endogenous control *rpoB*. Percentages indicate the level of repression of the operon (expression levels of *pfp* in cells with non-targeting pFR56apm *vs.* in cells carrying pFR56apm targeting the *pfp-ifp* operon). Error bars represent the standard error of the mean

($n = 2$ biological replicates, each as the median of 3 technical replicates). **C** Effect of CRISPRi repression on the growth of plasmid-free, pOXA-48- and pOXA-48ΔlysR-carrying KPN15. Individual points show independent replicates ($n = 16$). Asterisks represent statistical significance of two-way ANOVA and post hoc Tukey's tests (Supplementary Data 11): * $P \leq 0.05$, ** $P \leq 0.01$, *** $P \leq 0.001$. In boxplots (A) and (C), horizontal lines inside boxes indicate median values, upper and lower hinges correspond to the 25th and 75th percentiles, and whiskers extend to observations within the 1.5x the interquartile range. Source data are provided as a Source Data file.

enterobacterial hosts. These strains belong to four different clinically relevant species and are natural or sympatric hosts of pOXA-48^{13,42}. By integrating transcriptomic analyses with experimental work, we showed that a pOXA-48-encoded transcriptional regulator, *LysR_{pOXA-48}*, mediates a transcriptional crosstalk between the plasmid and the chromosome of *Klebsiella* spp. and *C. freundii* (Figs. 3A and 4A). Specifically, *LysR_{pOXA-48}* directly increases the expression of a small chromosomal operon comprised of the *pfp* and *ifp* genes (Figs. 3A, 4D and 5). This operon is present in many species of Proteobacteria and shows signs of having been horizontally acquired (Fig. 3B, C). Importantly, our results suggest that the overexpression of the operon leads to a growth benefit for pOXA-48-carrying *K. pneumoniae* KPN15 (Fig. 7C), and could therefore promote plasmid maintenance and transmission in clinical strains. In line with this hypothesis, we identified a strong association between the presence of the *pfp-ifp* operon and pOXA-48 carriage in a database of enterobacterial genomes. This finding supports our experimental results on the fitness advantage of *pfp-ifp* overexpression on pOXA-48 carriers. While it is true that *E. coli*, the second enterobacterial species most frequently associated with pOXA-48, does not typically encode the *pfp-ifp* operon, this association could be due to the fact that *E. coli* is the most prevalent enterobacteria in the human gut⁵⁶, and thus is more likely to acquire the

plasmid. Moreover, the distribution of pOXA-48 in enterobacteria can be influenced by multiple factors, like defense systems, as has been recently described for certain *E. coli* lineages⁵⁷.

A growing number of studies have reported plasmid-chromosome crosstalks mediated by plasmid-encoded regulators^{14,28}. However, there are only a few documented cases of crosstalks mediated by AMR plasmids^{38,40,41}. In this framework, our work is relevant for multiple reasons. First, we studied clinically relevant MDR carbapenemase-producing enterobacteria, which are consistently listed as the top critical group of bacterial pathogens by the World Health Organization⁵⁸. Second, we showed that this crosstalk occurs in MDR enterobacteria of different genera (*Klebsiella* and *Citrobacter*). Third, we performed a thorough analysis of the origin of the *lysR-pfp-ifp* cluster and provided evidence that it is mobilizable, highlighting the relevance of interactions between mobile genetic elements in AMR evolution^{16,59}. Finally, we characterized the regulatory activity of *LysR_{pOXA-48}* and the function of the *pfp-ifp* operon in depth, producing a pOXA-48 *lysR* deletion mutant and combining transcriptomic analyses with CRISPRi silencing. However, our study has limitations. First, experimental results were not fully reproducible between the *C. freundii* CF13 and *K. pneumoniae* KPN15 strains. This could be explained by the fact that these strains belong to different genera and

that CF13, unlike KPN15, was isolated carrying pOXA-48 and could therefore be adapted to carriage of the plasmid. Second, due to experimental constraints, we only tested the positive epistatic effect between pOXA-48 and the *pfp-ifp* operon overexpression in one strain (Fig. 7C). Finally, although CRISPRi results suggested that the overexpression of the *pfp-ifp* operon is beneficial in a pOXA-48-carrying strain, we could only partially reproduce the growth benefit associated with the overexpression of the *pfp-ifp* operon in pOXA-48Δ*lysR*-carrying strains. One possible explanation for this result is that the positive interaction between *pfp-ifp* operon overexpression and pOXA-48 only occurs at a narrow range of *lysR*_{pOXA-48} expression. However, it is also possible that there are relevant factors involved in this plasmid-chromosome crosstalk that we are not taking into consideration, such as potential effectors modulating the function of *LysR*_{pOXA-48}⁶⁰.

The specific plasmid-chromosome crosstalk described here may be unique to pOXA-48 and the *pfp-ifp* operon due to the unusual origin of the *LysR* encoded on the plasmid. It is well accepted that the *lysR* gene was mobilized, along with the carbapenemase gene, from the chromosome of *Shewanella* spp. into an IncL plasmid backbone, trapped within a Tn1999 composite transposon^{9,10}. Thus, it is not a common gene present in IncL plasmids, which may explain the epidemiological success of pOXA-48 (173 of 307 IncL plasmids in the RefSeq database were identified as pOXA-48). This transposition into pOXA-48 and the resulting plasmid-chromosome crosstalk could have initially been accidental. However, it is tempting to speculate that the presence of *lysR* on pOXA-48 could have been selected due to the beneficial effects of the crosstalk. Accordingly, throughout the evolution of pOXA-48, the function of *LysR* has remained largely unaffected—mutations affecting gene function are not common, and 7 out of 9 versions of Tn1999, including the most frequent ones, maintain the *lysR* intact (see Supplementary Information and Supplementary Fig. 22)^{9,13,61–63}. However, there is still much to understand about the functional and biological significance of the *LysR*_{pOXA-48} - *pfp-ifp* operon crosstalk, which will require further characterization.

Bacterial operons usually encode genes sharing similar or complementary biological functions⁶⁴, and we propose that this could be the case of the *pfp* and *ifp* genes. We showed that the PFP of *K. pneumoniae* KPN15 possesses quercetinase activity (Fig. 6A and Supplementary Figs. 13 and 14). Quercetin is a flavonoid present in many vegetables and is often consumed in the diet^{52,65}. Given its iron-chelating properties, quercetin could reduce the bioavailability of iron—a key growth and virulence factor—for gut enterobacteria⁶⁵. We hypothesized that the IFP, being in the same functional family as the EntB isochorismatase, could be involved in the biosynthesis of enterobactin, a high affinity siderophore⁵³. Thus, overexpression of the *pfp-ifp* operon by *LysR*_{pOXA-48} could lead to an increased enterobactin-mediated iron uptake by increasing the biosynthesis of enterobactin (IFP) and the bioavailability of iron—degrading the iron-chelating quercetin (PFP)—. However, we could not demonstrate any growth difference between pOXA-48- and pOXA-48Δ*lysR*-carrying strains in iron-deficient conditions (Supplementary Fig. 17). It is possible that the overexpression of other iron uptake systems observed in pOXA-48Δ*lysR*-carrying strains compared to the pOXA-48-carrying ones is compensating for the presence of the iron chelator (Fig. 6B, C and Supplementary Fig. 16). However, we could not rule out the possibility that the *pfp-ifp* operon has a different function, unrelated to iron uptake. For example, PFP could simply reduce susceptibility to quercetin, which has known antimicrobial properties⁵². Future work will help to uncover the role of this mysterious operon.

In summary, our study uncovers a plasmid-chromosome crosstalk that could facilitate the acquisition of carbapenem resistance in one of the most concerning groups of clinical pathogens, MDR enterobacteria. These results highlight, once again, the key role of plasmids as catalysts for bacterial adaptation beyond being mere drivers of horizontal gene transfer⁶⁶. Given the central role that plasmids play in

the dissemination of AMR, characterizing the complex interactions between these mobile genetic elements and their bacterial hosts seems crucial to understanding AMR evolution. Ultimately, we may be able to exploit these interactions to develop new intervention strategies against the increasing threat of AMR.

Methods

Bacterial strains

We selected a subsample of MDR strains from the R-GNOSIS collection, recovered in the Ramón y Cajal University Hospital during an active surveillance-screening programme for detecting and isolating ESBL/carbapenemase-producing Enterobacteriaceae from hospitalized patients (approved by the Hospital's Ethics Committee, Reference 251/13⁶⁷). All strains selected meet the European Centre for Disease Prevention and Control (ECDC) and the Centers for Disease Control and Prevention (CDC)'s conditions for qualifying as MDR Enterobacteriaceae: non-susceptible to ≥1 antimicrobial agent in >3 antimicrobial categories^{13,42,68}.

Strains of *Escherichia coli* C325 (ST137), *Citrobacter freundii* CF13 (ST22), *Klebsiella variicola* J57 (ST971) and *Klebsiella pneumoniae* H53 and K147 (ST487 and ST11, respectively) naturally carried plasmid pOXA-48. In a previous work, the genomes of these five strains were sequenced and closed (BioProject PRJNA626430) and isogenic pOXA-48-free clones were obtained by curing the plasmid⁴³. These strains were selected based on their representativeness of MDR enterobacteria in the hospital (see below), and on their compatibility with the CRISPR-Cas9 curing system⁴³. Strains of *E. coli* EC10 (ST69) and *K. pneumoniae* KPN04, KPN07 and KPN10 (ST1427) and KPN15 and KPN18 (ST11) did not carry pOXA-48, but were recovered from the same pool of patients, so we defined them as sympatric (ecologically compatible with it). pOXA-48-carrying transconjugants from these strains were obtained before^{42,69}. These 11 MDR strains were representative of the enterobacteria phylogenetic diversity in the R-GNOSIS collection (chosen from the most common PFGE profiles^{67,70,71}), and thus of gut colonization of hospitalized patients in the Hospital, and of pOXA-48 distribution of fitness effects (Supplementary Fig. 1)^{42,43}. Additionally, we included the laboratory-adapted *E. coli* MG1655, for which the pOXA-48-transconjugant was obtained before⁴⁴. Experiments and analyses with pOXA-48Δ*lysR* were performed with KPN15—selected due to belonging to the clinically relevant ST11 and showing a small number of mutations between the pOXA-48-free and transconjugant strain—and CF13. See Supplementary Data 1 for details.

Plasmids used in this study

The plasmid pOXA-48Δ*lysR* was built by interrupting the pOXA-48-encoded *lysR* gene with an *aph(3)-Ila* kanamycin-resistance cassette. This plasmid was built using lambda Red recombination as described in ref. 72. First, a cassette carrying the *aph(3)-Ila* gene and 500 bp left and right homology regions was cloned into plasmid pMP7⁷³ using Gibson Assembly. The cassette was amplified from the resulting pMP7-HR-kan-HR plasmid. The primers used in this construction and a more complete description on how pMP7-HR-kan-HR was built can be found in Supplementary Data 1. The pTet-*LysR* plasmid was built using Gibson Assembly. The primers can be found in Supplementary Data 1.

The plasmid pFR56apm was used for expression of the CRISPRi machinery. This plasmid is based on pFR56⁷⁴, with the chloramphenicol-resistance marker substituted by an apramycin-resistance gene. pFR56apm expresses dCas9 under the inducible promoter pHlf, and the single guide RNA + scaffold under a constitutive promoter. Two versions of the plasmid were used in this study: (i) a non-targeting control, with 20 random nucleotides as sgRNA that don't target anything in the chromosome of the strains, and (ii) a version that allows for silencing of the *pfp-ifp* operon, constructed as described in the original pFR56 paper and chosen out of all possible guides against *pfp* using a guide activity predictor⁵⁴. The

primers used for the construction of the pFR56apm versions are described in Supplementary Data 1.

Genomic analyses

Whole genome sequencing. The genomes of the six pOXA-48 MDR transconjugants and the *E. coli* MG1655 transconjugant were sequenced with long-read technology to generate closed sequences to use as references for the transcriptomic analyses. DNA extraction was performed as in ref. 75. Genomic DNA was sequenced at the Microbial Genome Sequencing Center (MiGS; Pittsburgh, PA, USA) using Nanopore technology or in-house with a MinION Mk1B as in ref. 75. Illumina reads of the six MDR transconjugants were obtained before (BioProject PRJNA641166)⁴² or were resequenced at MiGS with NextSeq 2000, generating 150 bp paired-end reads. The pOXA-48-carrying MG1655 strain was sequenced at MicrobesNG (Birmingham, UK) with a MiSeq, generating 250 bp paired-end reads.

Closing reference genomes. Quality control of Illumina reads was performed with FastQC v0.11.9 (<https://www.bioinformatics.babraham.ac.uk/projects/fastqc/>). Illumina reads of the six MDR transconjugants were processed with Trim Galore v0.6.4 (Cutadapt v2.8, <https://github.com/FelixKrueger/TrimGalore>) to trim ends with Phred quality scores lower than 20 and remove adapters and reads shorter than 50 bp. Reads of pOXA-48-carrying MG1655 were pre-processed by MicrobesNG. Hybrid assemblies were obtained with Unicycler v0.4.9⁷⁶ using the Illumina reads from ref. 42 and MicrobesNG and the Nanopore reads from MiGS. The assemblies of pOXA-48-carrying KPN04, KPN07 and KPN18 were fragmented, possibly due to short- and long-reads originating from different DNA extractions. Thus, Illumina reads from MiGS and long-reads generated in-house were used to generate new hybrid assemblies with Unicycler. These assemblies were complete except for a plasmid that could not be closed in pOXA-48-carrying KPN04 and KPN18. To close the plasmid, Nanopore reads were processed with filtlong v0.2.1 (<https://github.com/rwrick/filtlong>) to obtain a subset of high identity reads with a minimum read depth of 85x and filtered reads were assembled with Flye v2.9⁷⁷. Resulting assemblies were polished with Medaka v1.4.3 (<https://github.com/nanoporetech/medaka>) and several rounds of Pilon v1.24⁷⁸, mapping the trimmed Illumina reads until no more changes were made. Finally, polished assemblies were recircularized with circlator v1.5.5⁷⁹. This way, the incomplete plasmids from the Unicycler assemblies were replaced by the closed polished plasmids in the FASTA files. In pOXA-48-carrying EC10 and MG1655, the assembly of pOXA-48 was missing a 760 bp region affecting the first copy of *IS1* and a 90 bp region affecting the *traC* gene, respectively. However, these represent assembly errors because there were reads mapping to these regions when using the pOXA-48_K8 variant (accession number MT441554) as reference. Final reference genomes were annotated with PGAP v2021-07-01.build5508⁸⁰.

Phylogenetic tree of enterobacterial strains. Mashtree v1.2.0⁸¹ was used to generate a phylogenetic tree of mash distances between the closed genomes of the 12 pOXA-48-carrying strains, using a bootstrap of 100. The tree was represented with the Interactive Tree of Life (iTOL)⁸² online tool.

Transcriptomic analyses

RNA extraction, sequencing and quality control. RNA extraction was performed as in ref. 75. Briefly, cells were grown with continuous shaking in LB medium. When cultures reached an OD₆₀₀ of 0.5 (exponential phase), cells were collected at 4 °C, pelleted by centrifugation at 4 °C 12,000 g for 1 min and frozen immediately at -70 °C. Total RNA was purified from each sample using the NZY Total RNA Isolation kit (NZYTECH). RNA concentration was determined using the Qubit RNA Broad-Range Assay following the manufacturer's

instructions. Additionally, the quality of the RNA was examined using the Tape-Station system (Agilent). RNA was ribodepleted and sequenced at the Wellcome Trust Centre for Human Genetics (WTCHG; Oxford, UK) using the Illumina's NovaSeq6000 platform, resulting in >8 million reads per sample (first RNA-Seq dataset). Three biological replicates per strain and condition (carrying and not carrying pOXA-48) were sequenced, except for strains CF13, KPN10 + pOXA-48, KPN10 and MG1655 that only two replicates were sequenced due insufficient RNA Integrity number (RIN score). To further confirm and characterize the plasmid-chromosome crosstalk, another RNA extraction and sequencing was performed for strains CF13 and KPN15 carrying pOXA-48 or the pOXA-48Δ*lysR* variant (see the RT-qPCR Methods for the RNA extraction protocol). Total RNA (three biological replicates for each strain and condition) was ribodepleted and sequenced with the NextSeq2000 platform at SeqCoast Genomics (Portsmouth, NH, USA), generating >6 million reads per sample (second RNA-Seq dataset). The quality of the reads was checked with FastQC v0.11.9. Reads were trimmed, adapter-removed and filtered for length lower than 50 bp using Trim Galore v0.6.4.

Differential expression analysis. Trimmed reads were mapped to their corresponding reference genome with BWA-MEM v0.7.17⁸³. The percentage of mapped reads was >99% for all samples. The appropriate presence or absence of pOXA-48 in the replicates was confirmed by inspecting the read alignments. A replicate in pOXA-48-cured K147 and CF13 (first RNA-Seq dataset) actually carried the plasmid, so they were included as an additional replicate of the pOXA-48-carrying strains. The function *featureCounts* from the Rsubread v2.14.2 package⁸⁴ was used to obtain raw counts of reads mapping to each genomic feature (including CDS, ncRNA, tRNA, tmRNA, antisense RNA, RNase P and SRP RNA), with strand specificity. The percentage of alignments successfully assigned to features was >85%. The presence of all resident plasmids was confirmed by reads mapping to their respective references (raw counts). DE analysis was performed using DESeq2 v1.40.1⁸⁵ from raw counts by comparing the pOXA-48-carrying strains against their respective pOXA-48-free strains (first RNA-Seq dataset) or pOXA-48Δ*lysR*-carrying strains (second RNA-Seq dataset). Raw DEGs (log₂FC cutoff of 0 and adjusted *p*-value < 0.01) were filtered to obtain significant DEGs with an adjusted *p*-value < 0.05. Raw counts and significant DE results are available at S4 and Supplementary Data 10. For the interpretation of the DE of pOXA-48 genes in the comparison pOXA-48 *vs.* pOXA-48Δ*lysR* (second RNA-Seq dataset), genes nearing the *P_{cat}-aph(3)-IIa* insertion, including the *lysR* gene, were not considered due to possible polar effects. The Operon-mapper webserver (January 2023)⁸⁶ was used to determine whether the *pfp* and *ifp* genes formed a single operon.

Transcripts per million (TPM) calculation. TPM values were calculated from FPKM values computed with DESeq2 from raw counts. To plot pOXA-48 gene expression, TPM values of pOXA-48 genes were normalized by the median chromosomal TPM, since it shows lower coefficient of variance across samples (CV = 0.22) than the house-keeping genes *rpoD* (CV = 0.39), *dnaE* (CV = 0.50) or *recA* (CV = 0.46). TPM values are available at Supplementary Data 3.

Gene set enrichment analysis (GSEA). Raw DEGs from the first RNA-Seq dataset were annotated with Gene Ontology (GO) terms for biological processes (BP), molecular functions (MF) and cellular components (CC), retrieved from the UniProt database⁸⁷ on May 2023 by mapping the RefSeq IDs from the PGAP annotation files to UniProtKB IDs. The percentage of raw DEGs that were annotated with GO terms was >63%. It is important to note that the lack of functional annotations for a significant number of genes in a genome constitutes a general limitation of enrichment analyses, especially in microbial genomics. GSEA was performed for each strain on the lists of chromosomal and

plasmid raw DEGs, separately, ranked by \log_2FC (shrunk with DESeq2's *apeglm* method) with clusterProfiler v4.8.1⁸⁸, correcting for multiple tests with the Benjamini-Hochberg procedure (Supplementary Data 5).

Variant calling. To assess whether mutations accumulated in the chromosome or other plasmids during growth or construction of pOXA-48-, pOXA-48Δ*lysR*-carrying or pOXA-48-free samples affected gene expression, variant calling was performed on the transcribed regions with Snippy v4.6.0 (<https://github.com/tseemann/snippy>), using the RNA-Seq mappings obtained previously (–bam). Only mutations not present in all replicates per strain were considered, since mutations in all samples of a strain would not affect differential expression (Supplementary Data 2). Of the total 80 SNPs identified in transcribed regions, only 12 showed DE of the mutated gene (Supplementary Data 2). To confirm or discard suspected SNPs in plasmid pOXA-48, the RNA-Seq reads were mapped to the sequence of the pOXA-48_K8 variant (accession number MT441554), the variant that was introduced to the transconjugants (Supplementary Data 2).

Clustering of strains. To further analyze common transcriptomic responses between samples, 2,488 single copy orthologs (SCO; orthogroups which contain only one gene per strain) were identified with OrthoFinder v2.5.4⁸⁹. PCA (Supplementary Fig. 3A) and t-SNE (R package *Rtsne*, perplexity = 5; Supplementary Fig. 3B) were performed on the SCO of pOXA-48-carrying and -free replicates to visualize patterns of response to carriage of the plasmid. For this, total raw counts were first normalized with VST (variance stabilizing transformation; DESeq2 package) and subsetting of the SCO was performed afterwards. Hierarchical clustering (complete linkage method) was performed to find strains with similar DE profiles (Supplementary Fig. 3C).

Analysis of the *lysR-pfp-ifp* cluster

Identification of the *lysR-pfp-ifp* cluster in a database of Proteobacteria. To explore the origin of the *lysR-pfp-ifp* cluster, the protein sequences of the LysR, PFP and IFP were first searched in STRING⁹⁰. The conserved neighborhood view revealed the *lysR-pfp-ifp* cluster is present in different species across the Proteobacteria phylogeny (Supplementary Fig. 8). To further analyze the origin of the *lysR-pfp-ifp* cluster, all Proteobacteria RefSeq genomes with a “chromosome” or “complete” assembly level were downloaded from the NCBI database (retrieved on July 14th, 2023 from <https://www.ncbi.nlm.nih.gov/datasets/genome/>), which comprises 16,219 Gammaproteobacteria, 2,878 Betaproteobacteria, 2,441 Alphaproteobacteria, 1,086 Epsilonproteobacteria, 5 Deltaproteobacteria and 2 Zetaproteobacteria (Supplementary Data 7). A MacSyFinder v2.0 model⁹¹ was constructed to identify the *lysR-pfp-ifp* cluster in the Proteobacteria database. To construct the model, the Pfam HMM profiles (release 35.0)⁹² of the three proteins (LysR: PF03466, PFP: PF02678, IFP: PF00857) were downloaded from InterPro v95.0 after an InterProScan 5 search⁹³. The model, available at https://github.com/LaboraTORIBio/RNA-Seq_enterobacteria_pOXA-48, is configured to find systems that contain the three genes consecutively (min_mandatory_genes_required = 3, min_genes_required = 3, inter_gene_max_space = 0), although order and sense cannot be specified. Then, the model was used with MacSyFinder v2.1.1 to find the *lysR-pfp-ifp* cluster in the database. The MacSyFinder results were filtered using in-house scripts to remove systems with incorrect gene order and orientation. Correct systems were defined as having the gene order *lysR-pfp-ifp* or *lysR-ifp-pfp*, with *pfp* and *ifp* in the same strand and *lysR* in antisense, so that *lysR* is likely to control the expression of *pfp* and *ifp*. Also, in strains with more than one system detected (24 Gamma-, 32 Beta- and 18 Alphaproteobacteria), only the system encoding the *lysR* with higher percentage of protein sequence identity with the *lysR* of pOXA-48 (BLASTp v2.11.0 search⁹⁴) was kept. After filtering, 5,983 Gamma-, 191 Beta- and 172 Alphaproteobacteria strains encoded the *lysR-pfp-ifp* cluster. A

second MacSyFinder model excluding the LysR HMM profile was constructed (min_mandatory_genes_required = 2, min_genes_required = 2, inter_gene_max_space = 0) to assess whether there are *pfp-ifp* gene clusters without the associated *lysR* gene. Then, 132 Gamma-, 44 Beta-, 14 Alpha- and 3 Epsilonproteobacteria strains encoded only a *pfp-ifp* cluster without an adjacent *lysR* gene (strains encoding the *lysR-pfp-ifp* cluster and an additional *pfp-ifp* cluster are excluded from the count). Of these, 61 Gamma-, 15 Beta- and 8 Alphaproteobacteria strains encoded a *lysR* gene within ±2 genes distance from *pfp-ifp*, which was disrupted or frameshifted in 41 Gamma-, 5 Beta- and 3 Alphaproteobacteria strains—thus not identified by the first MacSyFinder model.

Phylogenetic tree of the *lysR-pfp-ifp* cluster. To reduce the size of the database of Proteobacteria encoding the *lysR-pfp-ifp* cluster, the concatenated protein sequences of the cluster (in the order *lysR-pfp-ifp*) were clustered using USEARCH v11.0.667⁹⁵ with a 0.99 identity threshold to avoid losing evolutionary information. The LysR, PFP and IFP protein sequences of the 698 representative strains of each resulting cluster were aligned with MAFFT v7.453⁹⁶. Alignments were trimmed with trimAl v1.4⁹⁷ and concatenated with catfasta2phyml (<https://github.com/nylander/catfasta2phyml>) for constructing the tree of the *lysR-pfp-ifp* cluster. Four phylogenetic trees (*lysR-pfp-ifp* cluster [Fig. 3B], LysR [Supplementary Fig. 9], PFP [Supplementary Fig. 10] and IFP [Supplementary Fig. 11]) were constructed with IQ-TREE v1.6.12⁹⁸ with best evolutionary model selection and 1000 ultra-fast bootstrap. Trees were visualized and edited with iTOL⁸².

Ancestral character reconstruction (ACR). To construct a phylogenetic tree of Gamma-, Beta- and Alphaproteobacteria for ACR, including strains encoding and lacking the *lysR-pfp-ifp* cluster, the database had to be reduced. The 698 representative *lysR-pfp-ifp* cluster-encoding strains (comprising 321 different species) were selected. From these 321 species, 138 species included strains encoding or lacking the *lysR-pfp-ifp* cluster. To include these events in ACR, 102 random strains from 102 species that had <10 strains not encoding the *lysR-pfp-ifp* cluster, and 180 random strains from 36 species (5 per species) that had ≥10 strains not encoding the *lysR-pfp-ifp* cluster were selected. Additionally, 35% of the remaining strains lacking the *lysR-pfp-ifp* cluster were selected (359 Gamma-, 131 Beta- and 234 Alphaproteobacteria). Finally, 10 random Epsilonproteobacteria strains were selected as outgroups. Thus, in total, 1,714 strains were selected. The phylogenetic tree of Proteobacteria was constructed from 128 conserved bacterial single-copy genes, described in ref. 99 and curated in ref. 100. These genes were identified in the 1,714 genomes using the Pfam HMM profiles (release 35.0) with a HMMER v3.3 (option –cut ga)¹⁰¹ search. Hits were filtered by score using the cutoffs reported in ref. 99, resulting in 125 gene markers present in >85% of strains. Protein sequences of each family were aligned with MAFFT (option –auto) and alignments were trimmed and concatenated with trimAl and catfasta2phyml. The tree was constructed with IQ-TREE as before (–m MFP –bb 1000) and rooted at the Epsilonproteobacteria clade with iTOL. Four rogue taxa were identified with TreeShrink v1.3.9¹⁰² and iTOL was used to prune the tree, removing the rogue taxa and 14 Gammaproteobacteria strains (none encoding the *lysR-pfp-ifp* cluster) that branched outside of the Gamma/Betaproteobacteria clade (Supplementary Fig. 20). ACR was performed with PastML v1.9.34¹⁰³ with default parameters, using the pruned tree and a table of presence/absence of the *lysR-pfp-ifp* cluster (Supplementary Fig. 12).

Genomic neighborhood of the *lysR-pfp-ifp* cluster. To analyze the regions upstream and downstream the *lysR-pfp-ifp* cluster, a subset of relevant and representative species was selected: 19 Enterobacteriaceae strains (including the Enterobacteriaceae strains that branched outside the Enterobacteriaceae clade, Fig. 3B) and other 5 Gamma-, 4 Beta- and 3 Alphaproteobacteria strains (Supplementary Fig. 13).

Except for the rogue Enterobacteriaceae strains and the strains used in this study, the remaining strains were randomly selected. Strains from the same species were selected so that they were distant on the phylogenetic tree (Fig. 3B). First, the regions 10 Kbp upstream and 10 Kbp downstream of the *lysR-pfp-ifp* cluster were extracted using the samtools v.1.14 *faidx* command¹⁰⁴. To obtain annotation files compatible with clinker, the fasta files of these regions were annotated with Prokka v.1.14.6¹⁰⁵ using the original annotated proteins as first priority (--proteins flag). The GBK files provided by Prokka were used as input for clinker v.0.0.28¹⁰⁶, executed with default parameters (i.e. minimum alignment sequence identity = 0.3). Two static HTML documents were plotted: one for all the 31 strains selected (Supplementary Fig. 13), and another with non-redundant representative strains ($n = 8$; Fig. 3C). In Fig. 3C, genes were colored based on the main functional groups identified (e.g. iron uptake) as well as on the potential relatedness to HGT (tRNAs and transposases).

CG content and codon adaptation index (CAI). The GC content and CAI was computed for the subset of non-redundant *lysR-pfp-ifp* cluster-encoding Proteobacteria ($n = 8$) to assess whether the *lysR-pfp-ifp* cluster showed further signs of horizontal acquisition. The GC content of the chromosome and the *lysR-pfp-ifp* cluster (from the start of *lysR* to the end of the second operon gene) were calculated as the ratio of GC nucleotides by the total nucleotides of the region (Supplementary Data 8). Codon usage compatibility was assessed by comparing the CAI of the *lysR-pfp-ifp* cluster genes to the median CAI of genes encoding for ribosomal proteins, which are highly expressed and thus have an optimized codon usage. First, a codon usage table was created from genes encoding for ribosomal proteins (retrieved from annotation files searching for the term “ribosomal protein”) using the *cusp* function of EMBOSS v6.6.0.0¹⁰⁷. The CAI of each *lysR-pfp-ifp* cluster gene and each ribosomal protein gene was computed using the *cai* function of the EMBOSS package, using the codon usage table previously created (Supplementary Data 8).

Association analysis. To study the possible association between encoding a *lysR-pfp-ifp* cluster and carrying pOXA-48 in the RefSeq database, pOXA-48 plasmids were first identified. A strain was considered to carry pOXA-48 when (i) the best, largest BLASTn hit between the sequence of pOXA-48 K8 (accession number MT441554) and the target contig had >95% identity and >10 Kb alignment, (ii) the contig contained the pOXA-48 IncL replicon and (iii) the *bla*_{OXA-48} gene, as detected by ABRicate with the PlasmidFinder and ResFinder databases. In total, 173 strains met these criteria, including 123 *Klebsiella* spp., 27 *E. coli*, 9 *Enterobacter* spp., 8 *Citrobacter* spp., 5 *Salmonella enterica* and 1 *Serratia marcescens* strains. Analyses were then performed with the RefSeq genomes of the six genera where pOXA-48 was identified ($n = 8125$ strains). Of these, 4728 strains encoded the *lysR-pfp-ifp* cluster, of which 145 carried pOXA-48. Additionally, 24 strains encoding the cluster with a non-functional *LysR* (*lysR* was disrupted or frameshifted) were also included, since the plasmid-chromosome crosstalk could still be possible. None of the latter carried pOXA-48. Associations were analyzed building 2×2 contingency tables and using the χ^2 test with Yates' continuity correction.

RT-qPCR

Bacterial RNA extraction. Overnight bacterial cultures grown in LB were diluted to 1:1000 in fresh medium. When necessary, LB medium was supplemented with anhydrotetracycline (aTc) 0.3 μ g/mL or 2,4-diacetylphloroglucinol (DAPG) 50 μ M. Cultures were grown in aerobic conditions at 37 °C with agitation until an OD₆₀₀ of 0.2–0.3 was reached. Then, 3 mL of each culture were pelleted (11,000 rpm, 1 min) to perform total RNA extraction (using BioRad's Aurum™ Total RNA Mini Kit). RNA concentration and purity were assessed using a nanodrop and all samples shown to have A260/A280 and A260/A230 ratios

≥ 2 . RNA integrity and lack of contamination by residual genomic DNA were evaluated by electrophoresis in a 1% agarose gel. All samples had intact 16S and 23S ribosomal RNA. Two or three biological replicates were obtained per group.

Reverse transcription (RT). RT was carried out for each replicate using 1 μ g of RNA as template and the High-Capacity cDNA Reverse Transcription Kit with RNase Inhibitor from Applied Biosystems.

qPCR. To quantify expression levels of *lysR*_{pOXA-48}, *bla*_{OXA-48}, *pfp* and *rpoB* (endogenous control), 2 μ L of the previous undiluted cDNA were used as template in a 20 μ L-reaction containing NZYSupreme qPCR Green Master Mix from Nzytech and the specific primer-pairs for each of the genes (Supplementary Data 1). Fluorescence data was measured using a 7500 Real-Time PCR System from Applied Biosystems. Relative mRNA quantities were calculated using the comparative threshold cycle (Ct) method and normalized using *rpoB* gene expression ($2^{-\Delta C_t}$). Efficiencies of each reaction were calculated by the standard curve method in triplicate (*bla*_{OXA-48}: Efficiency = 0.95, R² = 0.99; *lysR*_{pOXA-48}: Efficiency = 0.98, R² = 0.99; *pfp*: Efficiency = 0.97, R² = 0.99; *rpoB*: Efficiency = 0.98, R² = 0.99). Two independent experiments in triplicate were performed.

Evaluation of the antimicrobial effect of quercetin by the broth microdilution method

The susceptibility to quercetin of pOXA-48-carrying strains versus pOXA-48 Δ *lysR*-carrying strains was evaluated using the broth microdilution method. First, a quercetin dihydrate 10 mg/mL stock solution was prepared (97% purity Quercetin dihydrate from Fisher Scientific dissolved in DMSO from Sigma). Then, two-fold serial dilutions were performed in MH medium, starting at 128 μ g/mL and down to 1 μ g/mL. 100 μ L of the different dilutions were added per well to a 96-well microtiter plate. On top of that, a further 100 μ L of bacterial inoculum was added per well, obtained from a 1:2000 dilution of an overnight culture in MH medium (5×10^5 CFU/mL). The following controls were included: (i) a sterility control per dilution, where no bacterial inoculum was added, and (ii) a DMSO control prepared in the same way as the quercetin dilutions, to assess for the toxicity of DMSO alone. Growth curves (1 replicate for DMSO and 2 replicates for DMSO + QC, per concentration and strain) were performed by growing the cultures in a plate reader BioTek SynergyHTX for 24 h, at 37 °C with orbital shaking (282 cpm) and measuring the OD₆₀₀ every 10 min.

Iron chelator assays

Growth curves of plasmid-free, pOXA-48-carrying and pOXA-48 Δ *lysR*-carrying KPN15 and CF13 were performed in the presence of the Iron Chelator 2,2-Bipyridyl from VWR (ref. 30569.09). Concentrations of 2,2-Bipyridyl ranging from 0.016 mM to 0.5 mM were tested. Curves were performed from overnight cultures grown without 2,2-Bipyridyl and diluted down to 1:1000. Growth curves (3 replicates per condition and strain) were performed for 24 h, using a plate reader BioTek SynergyHTX, at 37 °C with orbital shaking (282 cpm) and measuring the OD₆₀₀ every 10 min.

Growth curves expressing *LysR*_{pOXA-48} in *trans*

Growth curves were performed to assess the effect of the overexpression of *LysR*_{pOXA-48} in plasmid-free KPN15 and CF13, as well as their pOXA-48- and pOXA-48 Δ *lysR*-carrying counterparts. Overexpression was performed in *trans* using pTet-*LysR* (*LysR*_{pOXA-48} under the control of the pTet promoter). Growth curves were started by diluting overnight cultures of each strain to a factor of 1:1000, in LB and LB supplemented with a range of aTc concentrations (0.075, 0.15 and 0.3 μ g/mL). Cultures were grown in a BioTek SynergyHTX plate reader, at 37 °C, for 24 h, measuring OD₆₀₀ every 10 min. Measurements were performed for 5 replicates of each strain/induced pairing.

Gene silencing through CRISPR interference (CRISPRi)

The two versions of pFR56apm (non-targeting control and the one targeting the *pfp-ifp* operon) were transformed into *E. coli* β 3914 θ + pTA-MOB^{108,109}. This strain is auxotrophic for diaminopimelic acid (DAP) and can be used as a counter-selectable donor strain. pTA-MOB allows for mobilization of pFR56, which carries an *oriT* but lacks the genes necessary for conjugation. This set-up was used for conjugation of the two versions of pFR56apm into plasmid-free CF13 and KPN15, and their pOXA-48- and pOXA-48 Δ lysR-carrying counterparts.

The resulting strains were grown overnight in LB supplemented with apramycin (50 μ g/mL), to select for pFR56, and DAPG (50 μ M), to induce *dcas9* expression. In the morning, an 1:1000 dilution was performed for each strain in LB supplemented with apramycin and DAPG, and cultures were grown in a BioTek's SynergyHTX plate reader, at 37 °C, for 24 h, measuring OD₆₀₀ every 10 min. Measurements were performed for 16 replicates of each strain.

Statistical analyses

All statistical analyses were performed with R v4.3.1 or v4.4.0 (www.R-project.org). Packages *ggplot2*, *ggpubr*, *ggfortify*, *cowplot*, *scales*, *heatmap*, *enrichplot*, *RColorBrewer*, *reshape2* and *tidyverse* were used for data representation and manipulation. R base and *car* packages were used for statistical tests. Normality and homoscedasticity of the data was assessed with the Shapiro-Wilk and Levene tests, respectively. Spearman's rank correlation was used for non-normal data. To compare means in the RT-qPCR results (see Fig. 4D), a one-way ANOVA (for KPN15, $F(2,3) = 165.4$, $P = 0.0009$; for CF13, $F(2,3) = 82.4$, $P = 0.002$) with two-tailed Dunnett's post hoc test, or two-tailed *t*-tests were used when appropriate. The area under the curve (AUC) of growth curves was computed with the R package *flux* v0.3.0.1. To compare growth differences in the pTet-LysR and CRISPRi assays (Fig. 7), two-sided two-way ANOVA and the post hoc Tukey's tests were performed (Supplementary Data 11). To assess the effect of the concentration of the drugs DMSO or DMSO + QC in growth (AUC, as the dependent variable), two GAMs were constructed for each strain (due to observable differences in growth and drug response) with the R package *mgcv* v1.9-1. A non-linear relationship was fitted per genotype (pOXA-48 or pOXA-48 Δ lysR) and drug (DMSO or DMSO + QC) interaction, including the interaction terms for both explanatory variables (formula: $AUC \sim s(\text{concentration}, k = 5, \text{by} = \text{genotype_drug}) + \text{genotype} * \text{drug}$). Genotype pOXA-48 Δ lysR and drug DMSO + QC were set as reference levels to obtain relevant comparisons. The Restricted Maximum Likelihood (REML) method was used. The optimal number of basis functions (*k*) was selected by comparing the model fit statistics (adjusted R-square, deviance explained and -REML; Supplementary Data 11).

Reporting summary

Further information on research design is available in the Nature Portfolio Reporting Summary linked to this article.

Data availability

Closed reference genomes are available at BioProjects [PRJNA626430](https://www.ncbi.nlm.nih.gov/bioproject/PRJNA626430) and [PRJNA1071971](https://www.ncbi.nlm.nih.gov/bioproject/PRJNA1071971) (see Supplementary Data 1). Genomic and transcriptomic sequencing data generated in this study is available at BioProject [PRJNA1071971](https://www.ncbi.nlm.nih.gov/bioproject/PRJNA1071971). Raw data generated during DE analysis can be found at the GEO Series [GSE269852](https://www.ncbi.nlm.nih.gov/geo/query/acc.cgi?acc=GSE269852). Source data are provided with this paper.

Code availability

Detailed bioinformatics workflows and the code produced in this study are available at https://github.com/LaboraTORlab/RNA-Seq-enterobacteria_pOXA-48.

References

- Murray, C. J. et al. Global burden of bacterial antimicrobial resistance in 2019: a systematic analysis. *Lancet* **399**, 629–655 (2022).
- O'Neill, J. Tackling Drug-Resistant Infections Globally: Final Report and Recommendations. <https://apo.org.au/node/63983> (2016).
- Gogarten, J. P. & Townsend, J. P. Horizontal gene transfer, genome innovation and evolution. *Nat. Rev. Microbiol.* **3**, 679–687 (2005).
- Smillie, C., Garcillán-Barcia, M. P., Francia, M. V., Rocha, E. P. C. & de la Cruz, F. Mobility of plasmids. *Microbiol. Mol. Biol. Rev.* **74**, 434–452 (2010).
- Baquero, F. et al. Evolutionary pathways and trajectories in antibiotic resistance. *Clin. Microbiol. Rev.* **34**, e00050–19 (2021).
- Bonomo, R. A. et al. Carbapenemase-producing organisms: a global scourge. *Clin. Infect. Dis. Publ. Infect. Dis. Soc. Am.* **66**, 1290–1297 (2018).
- Redondo-Salvo, S. et al. COPLA, a taxonomic classifier of plasmids. *BMC Bioinforma.* **22**, 390 (2021).
- Carattoli, A., Seiffert, S. N., Schwendener, S., Perreten, V. & Endimiani, A. Differentiation of IncL and IncM plasmids associated with the spread of clinically relevant antimicrobial resistance. *PLoS ONE* **10**, e0123063 (2015).
- Pitout, J. D. D., Peirano, G., Kock, M. M., Strydom, K.-A. & Matsuura, Y. The global ascendancy of OXA-48-type carbapenemases. *Clin. Microbiol. Rev.* **33**, e00102–e00119 (2019).
- Poirel, L., Bonnin, R. A. & Nordmann, P. Genetic features of the widespread plasmid coding for the carbapenemase OXA-48. *Antimicrob. Agents Chemother.* **56**, 559–562 (2012).
- Poirel, L., Héritier, C., Tolün, V. & Nordmann, P. Emergence of oxacillinase-mediated resistance to imipenem in *Klebsiella pneumoniae*. *Antimicrob. Agents Chemother.* **48**, 15–22 (2004).
- David, S. et al. Epidemic of carbapenem-resistant *Klebsiella pneumoniae* in Europe is driven by nosocomial spread. *Nat. Microbiol.* **4**, 1919–1929 (2019).
- León-Sampedro, R. et al. Pervasive transmission of a carbapenem resistance plasmid in the gut microbiota of hospitalised patients. *Nat. Microbiol.* **6**, 606–616 (2021).
- Billane, K., Harrison, E., Cameron, D. & Brockhurst, M. A. Why do plasmids manipulate the expression of bacterial phenotypes? *Philos. Trans. R. Soc. B* **377**, 20200461 (2022).
- Baltrus, D. A. Exploring the costs of horizontal gene transfer. *Trends Ecol. Evol.* **28**, 489–495 (2013).
- San Millan, A., Toll-Riera, M., Qi, Q. & MacLean, R. C. Interactions between horizontally acquired genes create a fitness cost in *Pseudomonas aeruginosa*. *Nat. Commun.* **6**, 6845 (2015).
- Harrison, E., Guymer, D., Spiers, A. J., Paterson, S. & Brockhurst, M. A. Parallel compensatory evolution stabilizes plasmids across the parasitism-mutualism continuum. *Curr. Biol.* **25**, 2034–2039 (2015).
- Lang, K. S. & Johnson, T. J. Transcriptome modulations due to A/C2 plasmid acquisition. *Plasmid* **80**, 83–89 (2015).
- Buckner, M. M. C. et al. Clinically relevant plasmid-host interactions indicate that transcriptional and not genomic modifications ameliorate fitness costs of *Klebsiella pneumoniae* carbapenemase-carrying plasmids. *mBio* **9**, e02303–e02317 (2018).
- Long, D. et al. Phenotypical profile and global transcriptomic profile of Hypervirulent *Klebsiella pneumoniae* due to carbapenemase-encoding plasmid acquisition. *BMC Genom.* **20**, 480 (2019).
- Lee, H. & Ko, K. S. Effect of multiple, compatible plasmids on the fitness of the bacterial host by inducing transcriptional changes. *J. Antimicrob. Chemother.* **76**, 2528–2537 (2021).
- Dunn, S., Carrilero, L., Brockhurst, M. & McNally, A. Limited and strain-specific transcriptional and growth responses to acquisition

- of a multidrug resistance plasmid in genetically diverse *Escherichia coli* lineages. *mSystems* **6**, e00083–21 (2021).
23. Element, S. J. et al. Growth in a biofilm promotes conjugation of a blaNDM-1-bearing plasmid between *Klebsiella pneumoniae* strains. *mSphere* **8**, e0017023 (2023).
 24. Hall, R. J., Snaith, A. E., Thomas, M. J. N., Brockhurst, M. A. & McNally, A. Multidrug resistance plasmids commonly reprogram the expression of metabolic genes in *Escherichia coli*. *mSystems* **9**, e0119323 (2024).
 25. Huang, C. et al. Comparative analysis of transcriptome and proteome revealed the common metabolic pathways induced by prevalent ESBL plasmids in *Escherichia coli*. *Int. J. Mol. Sci.* **24**, 14009 (2023).
 26. San Millan, A. & Craig MacLean, R. Fitness costs of plasmids: a limit to plasmid transmission. In *Microbial Transmission* 65–79 (John Wiley & Sons, Ltd, 2019). <https://doi.org/10.1128/9781555819743.ch4>.
 27. Hall, J. P. J. et al. Plasmid fitness costs are caused by specific genetic conflicts enabling resolution by compensatory mutation. *PLOS Biol.* **19**, e3001225 (2021).
 28. Vial, L. & Hommais, F. Plasmid-chromosome cross-talks. *Environ. Microbiol.* **22**, 540–556 (2020).
 29. Schaufler, K. et al. Carriage of extended-spectrum beta-lactamase-plasmids does not reduce fitness but enhances virulence in some strains of pandemic *E. coli* lineages. *Front. Microbiol.* **7**, 336 (2016).
 30. Jiang, X. et al. The CTX-M-14 plasmid pHK01 encodes novel small RNAs and influences host growth and motility. *FEMS Microbiol. Ecol.* **93**, 90 (2017).
 31. Thompson, C. M. A. et al. Plasmids manipulate bacterial behaviour through translational regulatory crosstalk. *PLOS Biol.* **21**, e3001988 (2023).
 32. Hüttner, M. et al. Expression of a novel class of bacterial Ig-like proteins is required for IncHI plasmid conjugation. *PLoS Genet.* **15**, e1008399 (2019).
 33. Lai, Y. C., Peng, H. L. & Chang, H. Y. RmpA2, an Activator of Capsule Biosynthesis in *Klebsiella pneumoniae* CG43, Regulates K2 cps Gene Expression at the Transcriptional Level. *J. Bacteriol.* **185**, 788 (2003).
 34. Chu, W. H. W. et al. Acquisition of regulator on virulence plasmid of hypervirulent *Klebsiella* allows bacterial lifestyle switch in response to iron. *mBio* (2023) <https://doi.org/10.1128/MBIO.01297-23>.
 35. Bourgogne, A., Drysdale, M., Hilsenbeck, S. G., Peterson, S. N. & Koehler, T. M. Global effects of virulence gene regulators in a *Bacillus anthracis* strain with both virulence plasmids. *Infect. Immun.* **71**, 2736–2743 (2003).
 36. Porter, M. E. et al. Direct and indirect transcriptional activation of virulence genes by an AraC-like protein, PerA from enteropathogenic *Escherichia coli*. *Mol. Microbiol.* **54**, 1117–1133 (2004).
 37. Coulson, G. B. et al. Transcriptome reprogramming by plasmid-encoded transcriptional regulators is required for host niche adaptation of a macrophage pathogen. *Infect. Immun.* **83**, 3137–3145 (2015).
 38. Di Venzio, G. et al. Urinary tract colonization is enhanced by a plasmid that regulates uropathogenic *Acinetobacter baumannii* chromosomal genes. *Nat. Commun.* **10**, 2763 (2019).
 39. Kloos, J., Gama, J. A., Hegstad, J., Samuelsen, Ø. & Johnsen, P. J. Piggybacking on niche adaptation improves the maintenance of multidrug-resistance plasmids. *Mol. Biol. Evol.* **38**, 3188–3201 (2021).
 40. Weber, H., Pesavento, C., Possling, A., Tischendorf, G. & Hengge, R. Cyclic-di-GMP-mediated signalling within the σ S network of *Escherichia coli*. *Mol. Microbiol.* **62**, 1014–1034 (2006).
 41. Benomar, S., Di Venzio, G. & Feldman, M. F. Plasmid-encoded H-NS controls extracellular matrix composition in a modern *Acinetobacter baumannii* urinary isolate. *J. Bacteriol.* **203**, e0027721 (2021).
 42. Alonso-del Valle, A. et al. Variability of plasmid fitness effects contributes to plasmid persistence in bacterial communities. *Nat. Commun.* **12**, 2653 (2021).
 43. Fernández-Calvet, A. et al. The distribution of fitness effects of plasmid pOXA-48 in clinical enterobacteria. *Microbiology* **169**, 001369 (2023).
 44. Rodríguez-Beltrán, J. et al. Translational demand is not a major source of plasmid-associated fitness costs. *Philos. Trans. R. Soc. B* **377**, 20200463 (2022).
 45. DelaFuente, J. et al. Within-patient evolution of plasmid-mediated antimicrobial resistance. *Nat. Ecol. Evol.* **6**, 1980–1991 (2022).
 46. Jousset, A. B. et al. Transcriptional landscape of a blaKPC-2 plasmid and response to imipenem exposure in *Escherichia coli* TOP10. *Front. Microbiol.* **9**, 2929 (2018).
 47. Allain, M. et al. Dissemination of IncI plasmid encoding bla CTX-M-1 is not hampered by its fitness cost in the pig's gut. *Antimicrob. Agents Chemother.* **67**, e00111–e00123 (2023).
 48. Rajer, F. & Sandegren, L. The role of antibiotic resistance genes in the fitness cost of multiresistance plasmids. *mBio* **13**, e0355221 (2022).
 49. Takahashi, Y. et al. Modulation of primary cell function of host *Pseudomonas* bacteria by the conjugative plasmid pCAR1. *Environ. Microbiol.* **17**, 134–155 (2015).
 50. Williams, K. P. Integration sites for genetic elements in prokaryotic tRNA and tmRNA genes: sublocation preference of integrase subfamilies. *Nucleic Acids Res.* **30**, 866–875 (2002).
 51. Adams, M. & Jia, Z. Structural and biochemical analysis reveal pirins to possess quercetinase activity. *J. Biol. Chem.* **280**, 28675–28682 (2005).
 52. Nguyen, T. L. A. & Bhattacharya, D. Antimicrobial activity of quercetin: an approach to its mechanistic principle. *Molecules* **27**, 2494 (2022).
 53. Raymond, K. N., Dertz, E. A. & Kim, S. S. Enterobactin: an archetype for microbial iron transport. *Proc. Natl Acad. Sci.* **100**, 3584–3588 (2003).
 54. Calvo-Villamañán, A. et al. On-target activity predictions enable improved CRISPR-dCas9 screens in bacteria. *Nucleic Acids Res.* **48**, e64 (2020).
 55. Vigouroux, A. & Bikard, D. CRISPR tools to control gene expression in bacteria. *Microbiol. Mol. Biol. Rev.* **84**, e00077–19 (2020).
 56. Martinson, J. N. V. et al. Rethinking gut microbiome residency and the Enterobacteriaceae in healthy human adults. *ISME J.* **13**, 2306–2318 (2019).
 57. Zongo, P. D. et al. An antiplasmid system drives antibiotic resistance gene integration in carbapenemase-producing *Escherichia coli* lineages. *Nat. Commun.* **15**, 4093 (2024).
 58. WHO Bacterial Priority Pathogens List, 2024: Bacterial Pathogens of Public Health Importance to Guide Research, Development and Strategies to Prevent and Control Antimicrobial Resistance. <https://www.who.int/publications/i/item/9789240093461> (2024).
 59. Horne, T., Orr, V. T. & Hall, J. P. How do interactions between mobile genetic elements affect horizontal gene transfer? *Curr. Opin. Microbiol.* **73**, 102282 (2023).
 60. Maddocks, S. E. & Oyston, P. C. F. Structure and function of the LysR-type transcriptional regulator (LTTR) family proteins. *Microbiol. Read. Engl.* **154**, 3609–3623 (2008).
 61. Sattler, J. et al. Emergence of Tn1999.7, a new transposon in blaOXA-48-harboring plasmids associated with increased plasmid stability. *Antimicrob. Agents Chemother.* **66**, e00787–22 (2022).

62. Potron, A., Poirel, L., Rondinaud, E. & Nordmann, P. Inter-continental spread of OXA-48 beta-lactamase-producing enterobacteriaceae over a 11-year period, 2001 to 2011. *Eur. Surveill.* **18**, pii=20549 (2013).
63. Lermineaux, N. et al. Plasmid genomic epidemiology of carbapenem-hydrolysing class D β -lactamase (CDHL)-producing Enterobacteriales in Canada, 2010–2021. *Microb. Genom.* **10**, 001257 (2024).
64. Osbourn, A. E. & Field, B. Operons. *Cell. Mol. Life Sci.* **66**, 3755–3775 (2009).
65. Scarano, A. et al. The chelating ability of plant polyphenols can affect iron homeostasis and gut microbiota. *Antioxidants* **12**, 630 (2023).
66. Rodríguez-Beltrán, J., DelaFuente, J., León-Sampedro, R., MacLean, R. C. & San Millán, Á. Beyond horizontal gene transfer: the role of plasmids in bacterial evolution. *Nat. Rev. Microbiol.* **19**, 347–359 (2021).
67. Hernández-García, M. et al. Characterization of carbapenemase-producing Enterobacteriaceae from colonized patients in a university hospital in Madrid, Spain, during the R-GNOSIS project depicts increased clonal diversity over time with maintenance of high-risk clones. *J. Antimicrob. Chemother.* **73**, 3039–3043 (2018).
68. Magiorakos, A.-P. et al. Multidrug-resistant, extensively drug-resistant and pandrug-resistant bacteria: an international expert proposal for interim standard definitions for acquired resistance. *Clin. Microbiol. Infect.* **18**, 268–281 (2012).
69. Alonso-del Valle, A. et al. Antimicrobial resistance level and conjugation permissiveness shape plasmid distribution in clinical enterobacteria. *Proc. Natl. Acad. Sci. USA.* **120**, e2314135120 (2023).
70. Díaz-Agero Pérez, C. et al. Local prevalence of extended-spectrum beta-lactamase (ESBL) producing Enterobacteriaceae intestinal carriers at admission and co-expression of ESBL and OXA-48 carbapenemase in *Klebsiella pneumoniae*: a prevalence survey in a Spanish University Hospital. *BMJ Open* **9**, e024879 (2019).
71. Maechler, F. et al. Contact isolation versus standard precautions to decrease acquisition of extended-spectrum β -lactamase-producing Enterobacteriales in non-critical care wards: a cluster-randomised crossover trial. *Lancet Infect. Dis.* **20**, 575–584 (2020).
72. Datsenko, K. A. & Wanner, B. L. One-step inactivation of chromosomal genes in *Escherichia coli* K-12 using PCR products. *Proc. Natl. Acad. Sci. USA.* **97**, 6640–6645 (2000).
73. Vit, C. et al. Cassette recruitment in the chromosomal Integron of *Vibrio cholerae*. *Nucleic Acids Res.* **49**, 5654–5670 (2021).
74. Rousset, F. et al. The impact of genetic diversity on gene essentiality within the *Escherichia coli* species. *Nat. Microbiol.* **6**, 301–312 (2021).
75. Sastre-Dominguez, J. et al. Plasmid-encoded insertion sequences promote rapid adaptation in clinical enterobacteria. *Nat. Ecol. Evol.* **8**, 2097–2112 (2024).
76. Wick, R. R., Judd, L. M., Gorrie, C. L. & Holt, K. E. Unicycler: Resolving bacterial genome assemblies from short and long sequencing reads. *PLoS Comput. Biol.* **13**, e1005595 (2017).
77. Kolmogorov, M., Yuan, J., Lin, Y. & Pevzner, P. A. Assembly of long, error-prone reads using repeat graphs. *Nat. Biotechnol.* **37**, 540–546 (2019).
78. Walker, B. J. et al. Pilon: An integrated tool for comprehensive microbial variant detection and genome assembly improvement. *PLoS ONE* **9**, e112963 (2014).
79. Hunt, M. et al. Circlator: automated circularization of genome assemblies using long sequencing reads. *Genome Biol.* **16**, 294 (2015).
80. Tatusova, T. et al. NCBI prokaryotic genome annotation pipeline. *Nucleic Acids Res.* **44**, 6614–6624 (2016).
81. Katz, L. S. et al. Mashtree: a rapid comparison of whole genome sequence files. *J. Open Source Softw.* **4**, 1762 (2019).
82. Letunic, I. & Bork, P. Interactive Tree Of Life (iTOL) v5: an online tool for phylogenetic tree display and annotation. *Nucleic Acids Res.* **49**, W293–W296 (2021).
83. Li, H. Aligning sequence reads, clone sequences and assembly contigs with BWA-MEM. Preprint at <https://doi.org/10.48550/arXiv.1303.3997> (2013).
84. Liao, Y., Smyth, G. K. & Shi, W. featureCounts: an efficient general purpose program for assigning sequence reads to genomic features. *Bioinformatics* **30**, 923–930 (2014).
85. Love, M. I., Huber, W. & Anders, S. Moderated estimation of fold change and dispersion for RNA-seq data with DESeq2. *Genome Biol.* **15**, 550 (2014).
86. Taboada, B., Estrada, K., Ciria, R. & Merino, E. Operon-mapper: a web server for precise operon identification in bacterial and archaeal genomes. *Bioinformatics* **34**, 4118–4120 (2018).
87. Consortium, UniProt UniProt: the Universal Protein Knowledge-base in 2023. *Nucleic Acids Res.* **51**, D523–D531 (2023).
88. Wu, T. et al. clusterProfiler 4.0: A universal enrichment tool for interpreting omics data. *Innovation* **2**, 100141 (2021).
89. Emms, D. M. & Kelly, S. OrthoFinder: phylogenetic orthology inference for comparative genomics. *Genome Biol.* **20**, 238 (2019).
90. Szklarczyk, D. et al. The STRING database in 2023: protein-protein association networks and functional enrichment analyses for any sequenced genome of interest. *Nucleic Acids Res.* **51**, D638–D646 (2023).
91. Abby, S. S., Néron, B., Ménager, H., Touchon, M. & Rocha, E. P. C. MacSyFinder: a program to mine genomes for molecular systems with an application to CRISPR-Cas systems. *PLOS ONE* **9**, e110726 (2014).
92. Mistry, J. et al. Pfam: The protein families database in 2021. *Nucleic Acids Res.* **49**, D412–D419 (2021).
93. Jones, P. et al. InterProScan 5: Genome-scale protein function classification. *Bioinformatics* **30**, 1236–1240 (2014).
94. Altschul, S. F., Gish, W., Miller, W., Myers, E. W. & Lipman, D. J. Basic local alignment search tool. *J. Mol. Biol.* **215**, 403–410 (1990).
95. Edgar, R. C. Search and clustering orders of magnitude faster than BLAST. *Bioinformatics* **26**, 2460–2461 (2010).
96. Katoh, K. & Standley, D. M. MAFFT multiple sequence alignment software version 7: improvements in performance and usability. *Mol. Biol. Evol.* **30**, 772–780 (2013).
97. Capella-Gutiérrez, S., Silla-Martínez, J. M. & Gabaldón, T. trimAl: a tool for automated alignment trimming in large-scale phylogenetic analyses. *Bioinforma. Oxf. Engl.* **25**, 1972–1973 (2009).
98. Nguyen, L.-T., Schmidt, H. A., von Haeseler, A. & Minh, B. Q. IQ-TREE: A fast and effective stochastic algorithm for estimating maximum-likelihood phylogenies. *Mol. Biol. Evol.* **32**, 268–274 (2015).
99. Rinke, C. et al. Insights into the phylogeny and coding potential of microbial dark matter. *Nature* **499**, 431–437 (2013).
100. d’Humières, C. et al. A simple, reproducible and cost-effective procedure to analyse gut phageome: from phage isolation to bioinformatic approach. *Sci. Rep.* **9**, 11331 (2019).
101. Eddy, S. R. Accelerated profile HMM searches. *PLOS Comput. Biol.* **7**, e1002195 (2011).
102. Mai, U. & Mirarab, S. TreeShrink: fast and accurate detection of outlier long branches in collections of phylogenetic trees. *BMC Genom.* **19**, 272 (2018).
103. Ishikawa, S. A., Zhukova, A., Iwasaki, W. & Gascuel, O. A fast likelihood method to reconstruct and visualize ancestral scenarios. *Mol. Biol. Evol.* **36**, 2069–2085 (2019).
104. Danecek, P. et al. Twelve years of SAMtools and BCFtools. *Giga-Science* **10**, giab008 (2021).

105. Seemann, T. Prokka: Rapid prokaryotic genome annotation. *Bioinformatics* **30**, 2068–2069 (2014).
106. Gilchrist, C. L. M. & Chooi, Y.-H. clinker & clustermap.js: automatic generation of gene cluster comparison figures. *Bioinformatics* **37**, 2473–2475 (2021).
107. Rice, P., Longden, I. & Bleasby, A. EMBOSS: the European Molecular Biology Open Software Suite. *Trends Genet. TIG* **16**, 276–277 (2000).
108. Le Roux, F., Binesse, J., Saulnier, D. & Mazel, D. Construction of a *Vibrio splendidus* mutant lacking the metalloprotease gene vsm by use of a novel counterselectable suicide vector. *Appl. Environ. Microbiol.* **73**, 777–784 (2007).
109. Strand, T. A., Lale, R., Degnes, K. F., Lando, M. & Valla, S. A new and improved host-independent plasmid system for RK2-based conjugal transfer. *PLoS One* **9**, e90372 (2014).

Acknowledgements

This work was supported by the European Research Council (ERC) under the European Union's Horizon 2020 research and innovation programme (ERC grant no. 757440-PLASREVOLUTION) and under the European Union's Horizon Europe research and innovation programme (ERC-2022-CoG Project 101086992 – PLAS-FIGHTER), by MCIN/AEI/10.13039/501100011033 and the European Union NextGenerationEU/PRTR (Project PCI2021-122062-2A) and by the Fundación Francisco Soria Melguizo (CC23140547). A.C.V. was funded by an EMBO postdoctoral fellowship (ALTF 322-2022). CH is supported by a Sara Borrell contract from the Carlos III Health Institute (ISCIII) (grant no. CD21/00115), the *Convocatoria Intramural Emergentes 2021* FIBioHRC-IRYCIS. Cod. IPM-21 n° C13, and PI23/01945 and MV23/00102 projects funded by Carlos III Health Institute (ISCIII). A.F.C. was funded by MCIN/AEI/10.13039/501100011033 and by the 'European Union NextGenerationEU/PRTR' (Grant FJC2021-046751-I). We thank David Bikard and the Institut Pasteur for the gift of plasmid pFR56.

Author contributions

L.T.C., A.C.V., C.H., A.F.C. and A.S.M. conceptualized the study. L.T.C., A.C.V., C.H., A.F.C. and A.S.M. designed the methodology. L.T.C. and J.S.D. performed the bioinformatic analyses. A.C.V., C.H., A.A.dV., S.Q. and A.F.C. performed the experiments. L.T.C., A.C.V., J.S.D., A.F.C. and A.S.M. contributed to data analysis. D.M. supervised experimental work. E.R. supervised bioinformatic analyses. A.S.M. was responsible for funding acquisition and supervision. L.T.C., A.C.V., A.F.C. and A.S.M.

wrote the original draft and undertook the reviewing and editing process. All authors supervised and approved the final version of the manuscript.

Competing interests

The authors declare no competing interests.

Additional information

Supplementary information The online version contains supplementary material available at <https://doi.org/10.1038/s41467-024-55169-y>.

Correspondence and requests for materials should be addressed to Ariadna Fernández-Calvet or Alvaro San Millán.

Peer review information *Nature Communications* thanks Michelle Buckner, and the other, anonymous, reviewer(s) for their contribution to the peer review of this work. A peer review file is available.

Reprints and permissions information is available at <http://www.nature.com/reprints>

Publisher's note Springer Nature remains neutral with regard to jurisdictional claims in published maps and institutional affiliations.

Open Access This article is licensed under a Creative Commons Attribution-NonCommercial-NoDerivatives 4.0 International License, which permits any non-commercial use, sharing, distribution and reproduction in any medium or format, as long as you give appropriate credit to the original author(s) and the source, provide a link to the Creative Commons licence, and indicate if you modified the licensed material. You do not have permission under this licence to share adapted material derived from this article or parts of it. The images or other third party material in this article are included in the article's Creative Commons licence, unless indicated otherwise in a credit line to the material. If material is not included in the article's Creative Commons licence and your intended use is not permitted by statutory regulation or exceeds the permitted use, you will need to obtain permission directly from the copyright holder. To view a copy of this licence, visit <http://creativecommons.org/licenses/by-nc-nd/4.0/>.

© The Author(s) 2024